Cell Metabolism

Article

Sustained alternate-day fasting potentiates doxorubicin cardiotoxicity

Graphical abstract

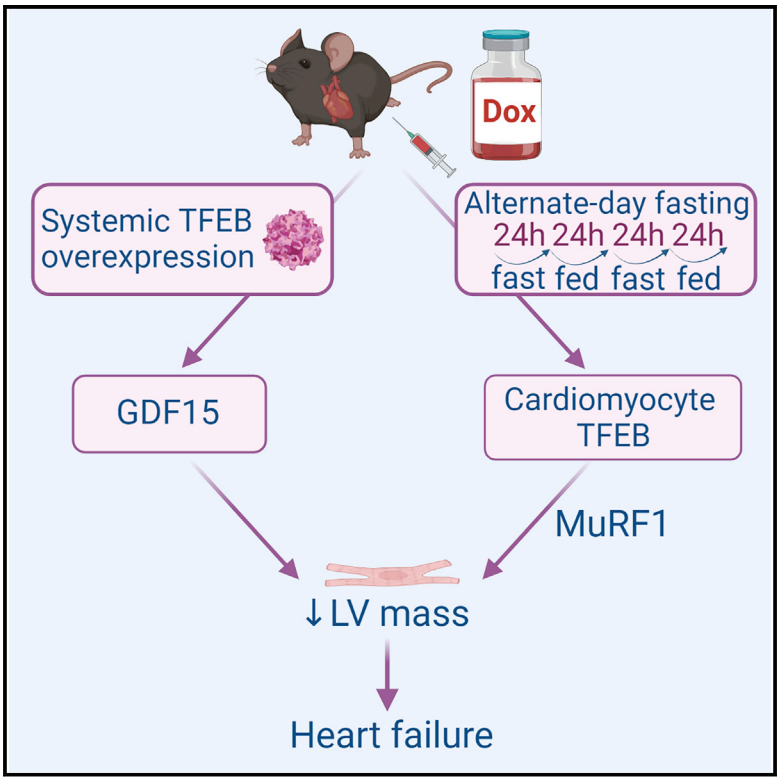

Authors

Mualla Ozcan, Zhen Guo, Carla Valenzuela Ripoll, ..., Babak Razani, Abhinav Diwan, Ali Javaheri

Correspondence

ali.javaheri@wustl.edu

In brief

Fasting strategies are under active clinical investigation in patients receiving chemotherapy. Ozcan, Guo, et al. identify that both sustained alternate-day fasting and a TFEB/GDF15 pathway potentiate doxorubicin-induced mortality and cardiotoxicity in mice.

Highlights

- TFEB levels are increased in end-stage doxorubicin-induced heart failure
- Sustained fasting and TFEB promote doxorubicin-induced cardiotoxicity
- TFEB increases GDF15, which is sufficient to reduce left ventricular mass
- In survivors of childhood cancer, left ventricular mass correlates with stroke volume

Ozcan et al., 2023, Cell Metabolism *35*, 1–15
April 4, 2023
https://doi.org/10.1016/j.cmet.2023.02.006

CellPress

Cell Metabolism

CellPress
OPEN ACCESS

Article

Sustained alternate-day fasting potentiates doxorubicin cardiotoxicity

Mualla Ozcan,[1,6] Zhen Guo,[1,6] Carla Valenzuela Ripoll,[1] Ahmed Diab,[1] Antonino Picataggi,[1] David Rawnsley,[1] Aynaz Lotfinaghsh,[1] Carmen Bergom,[1] Jeff Szymanski,[1] Daniel Hwang,[1] Aarti Asnani,[2] Mikhail Kosiborod,[3] Jie Zheng,[1] Robert J. Hayashi,[1] Pamela K. Woodard,[1] Attila Kovacs,[1] Kenneth B. Margulies,[4] Joel Schilling,[1] Babak Razani,[1,5] Abhinav Diwan,[1,5] and Ali Javaheri[1,7,8,*]

[1]Washington University School of Medicine, St. Louis, MO 63110, USA
[2]Beth Israel and Harvard Medical School, Boston, MA, USA
[3]St. Luke's Kansas City, Kansas City, MO, USA
[4]Perelman School of Medicine, University of Pennsylvania, Philadelphia, PA, USA
[5]John Cochran Veterans Affairs Medical Center, Saint Louis, MO, USA
[6]These authors contributed equally
[7]Twitter: @Alicardsdoc
[8]Lead contact
*Correspondence: ali.javaheri@wustl.edu
https://doi.org/10.1016/j.cmet.2023.02.006

SUMMARY

Fasting strategies are under active clinical investigation in patients receiving chemotherapy. Prior murine studies suggest that alternate-day fasting may attenuate doxorubicin cardiotoxicity and stimulate nuclear translocation of transcription factor EB (TFEB), a master regulator of autophagy and lysosomal biogenesis. In this study, human heart tissue from patients with doxorubicin-induced heart failure demonstrated increased nuclear TFEB protein. In mice treated with doxorubicin, alternate-day fasting or viral TFEB transduction increased mortality and impaired cardiac function. Mice randomized to alternate-day fasting plus doxorubicin exhibited increased TFEB nuclear translocation in the myocardium. When combined with doxorubicin, cardiomyocyte-specific TFEB overexpression provoked cardiac remodeling, while systemic TFEB overexpression increased growth differentiation factor 15 (GDF15) and caused heart failure and death. Cardiomyocyte TFEB knockout attenuated doxorubicin cardiotoxicity, while recombinant GDF15 was sufficient to cause cardiac atrophy. Our studies identify that both sustained alternate-day fasting and a TFEB/GDF15 pathway exacerbate doxorubicin cardiotoxicity.

INTRODUCTION

Cardiotoxicity and subsequent heart failure remain significant complications of anthracycline (doxorubicin or Dox) chemotherapy. One of the mechanistic hallmarks of Dox cardiotoxicity is autophagic impairment caused by lysosomal injury.[1] Intermittent fasting (IF) is a well-known stimulus for enhancing autophagic flux, and we previously have shown in mice that a type of IF called alternate-day fasting (ADF), with 24 h of fasting alternating with 24 h of feeding, rescues advanced forms of cardiomyopathy by stimulating nuclear translocation of transcription factor EB (TFEB), a master regulator of autophagy and lysosomal biogenesis.[2] A number of studies from our group[3] and others[4] have shown that fasting strategies, including ADF, ameliorate glucose intolerance that results from diet-induced obesity and mitigate myocardial injury via mechanisms that involve the autophagy-lysosome pathway.[2,5,6] Furthermore, Dox is known to acutely reduce TFEB nuclear levels,[7] and TFEB overexpression was suggested to ameliorate Dox cardiotoxicity.[8]

Based on this paradigm, ADF may attenuate anthracycline cardiotoxicity by restoring autophagy and increasing TFEB; however, recent studies of IF and time-restricted feeding have suggested loss of lean body mass,[9,10] although this is controversial.[11] Given that Dox causes loss of cardiac muscle mass in both mice and humans[12,13] and that in skeletal muscle, TFEB regulates the E3 ubiquitin ligase muscle RING-finger protein 1 (MuRF1),[14] which is implicated in muscle atrophy and Dox cardiotoxicity,[13] we sought to further investigate the roles of ADF and TFEB in Dox cardiotoxicity. Our findings suggest that TFEB is increased, rather than decreased, in human end-stage heart failure due to Dox and that a physiological (via ADF) or viral-mediated increase in TFEB provokes left ventricular (LV) atrophy and heart failure in mice. Decreased LV mass, seen in our models, correlates with reduced stroke volume, a finding we show is consistent across mice and humans. These data point to a previously unrecognized potential toxicity of sustained ADF and TFEB in the setting of Dox.

Please cite this article in press as: Ozcan et al., Sustained alternate-day fasting potentiates doxorubicin cardiotoxicity, Cell Metabolism (2023), https://doi.org/10.1016/j.cmet.2023.02.006

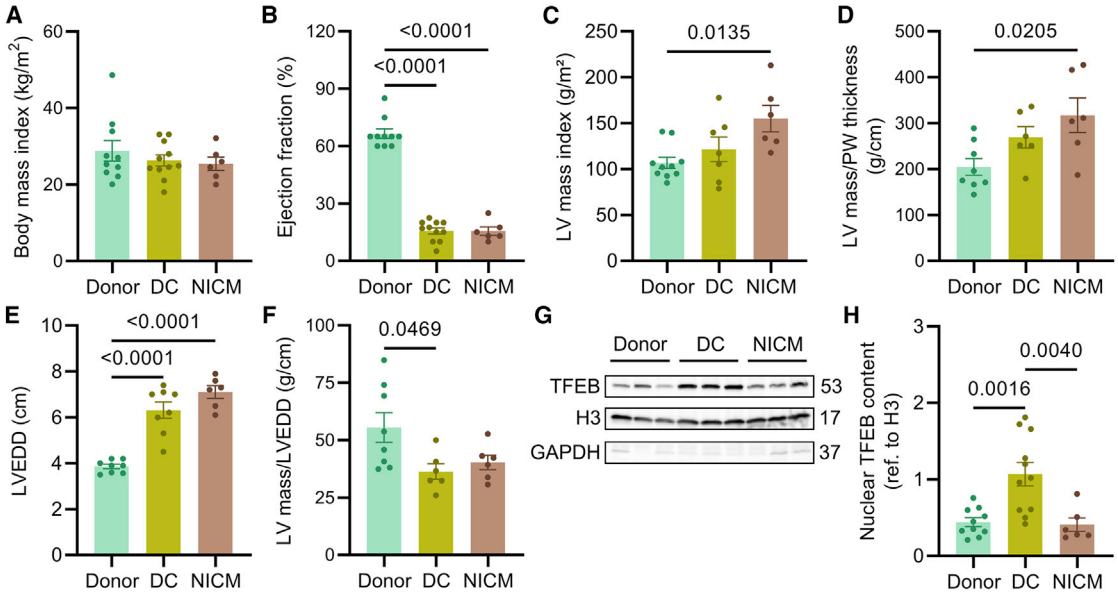

Figure 1. Myocardium from patients with doxorubicin cardiomyopathy demonstrates increased nuclear TFEB content

(A) Body mass index of donors (donor, n = 10), patients with a history of heart failure due to doxorubicin cardiomyopathy (DC, n = 11), and patients with non-ischemic dilated cardiomyopathy (NICM, n = 6) (one-way ANOVA, no significant difference).

(B) Ejection fraction of donor (n = 10), patients with DC (n = 11), and patients with NICM (n = 6) (one-way ANOVA with Šidák's correction for multiple comparisons).

(C) Left ventricular (LV) mass index of donor (n = 10), patients with DC (n = 7), and patients with NICM (n = 6) (one-way ANOVA with Šidák's correction for multiple comparisons).

(D) LV mass/posterior wall (PW) thickness of donor (n = 8), patients with DC (n = 6), and patients with NICM (n = 6) (one-way ANOVA with Šidák's correction for multiple comparisons).

(E) LV end-diastolic dimension (LVEDD) of donor (n = 8), patients with DC (n = 8), and patients with NICM (n = 6) (one-way ANOVA with Šidák's correction for multiple comparisons).

(F) LV mass/LVEDD of donor (n = 8), patients with DC (n = 6), and patients with NICM (n = 6) (one-way ANOVA with Šidák's correction for multiple comparisons).

(G) Representative immunoblots of TFEB in nuclear isolates of LV myocardial tissue from donor (n = 10), patients with DC (n = 11), and patients with NICM (n = 6). Histone H3 serves as a loading control, and GAPDH is shown to verify cytoplasmic protein removal.

(H) Quantification of immunoblots in (G) (one-way ANOVA with Šidák's correction for multiple comparisons).

All data are presented as mean ± SEM and analyzed by GraphPad Prism 9.0. Each dot represents one person in (A)–(F) and (H). Adjusted p values are shown in (B)–(F) and (H).

RESULTS

Myocardial tissue from patients with Dox-induced cardiomyopathy exhibits increased nuclear TFEB abundance

To explore the role of TFEB in human Dox cardiomyopathy (DC), we utilized samples from the University of Pennsylvania Tissue Bank and compared matched (1) patients with DC, (2) patients with non-ischemic cardiomyopathy (NICM) based on clinical characteristics, and (3) selected donor controls without a clinical history of heart failure. Donor and patients with NICM were selected who were non-diabetic, and patients with DC or NICM had no history of left ventricular assist devices (LVADs). Clinical characteristics are detailed in Table S1. Mean age was 58.3 ± 1.7, 47.45 ± 3.2, and 53.2 ± 4.2 years for donors, patients with DC, and patients with NICM, respectively. There were no significant differences in body mass index between groups (Figure 1A). Mean ejection fraction was significantly reduced in patients with DC and NICM, compared with donors (Figure 1B), while LV mass index (g/m^2) and LV mass/posterior wall (PW) thickness (g/cm) were significantly increased in patients with NICM vs. donors only (Figures 1C and 1D). Both patients with DC and patients with NICM exhibited increased LV dilation (Figure 1E), and patients with DC exhibited relatively greater concentric remodeling, based on the ratio of LV mass to end-diastolic dimension (Figure 1F). We performed nuclear protein isolation from patient samples (n = 6–11 per group), followed by immunoblotting for TFEB (Figure 1G). Based on the similarities in ejection fraction and dilation, and on prior murine data suggesting that Dox reduces TFEB nuclear abundance, we hypothesized that there is a reduced TFEB nuclear abundance in myocardium from patients with DC. By contrast, we observed that only the DC group exhibited an ~2.5-fold increase in nuclear TFEB abundance versus myocardial tissue from both donors and patients with NICM (Figure 1H).

ADF provokes mortality and cardiotoxicity in Dox-treated mice

ADF has previously been suggested as a therapeutic intervention that ameliorates Dox cardiotoxicity in mice,[15] based on the premise that ADF causes stimulation of autophagy and lysosomal biogenesis,[15] driven by pulsed activation of TFEB.[5] Given our observation of increased TFEB in myocardial tissue from patients with DC, we performed ADF in chow-fed male and female

Please cite this article in press as: Ozcan et al., Sustained alternate-day fasting potentiates doxorubicin cardiotoxicity, Cell Metabolism (2023), https://doi.org/10.1016/j.cmet.2023.02.006

CellPress
OPEN ACCESS

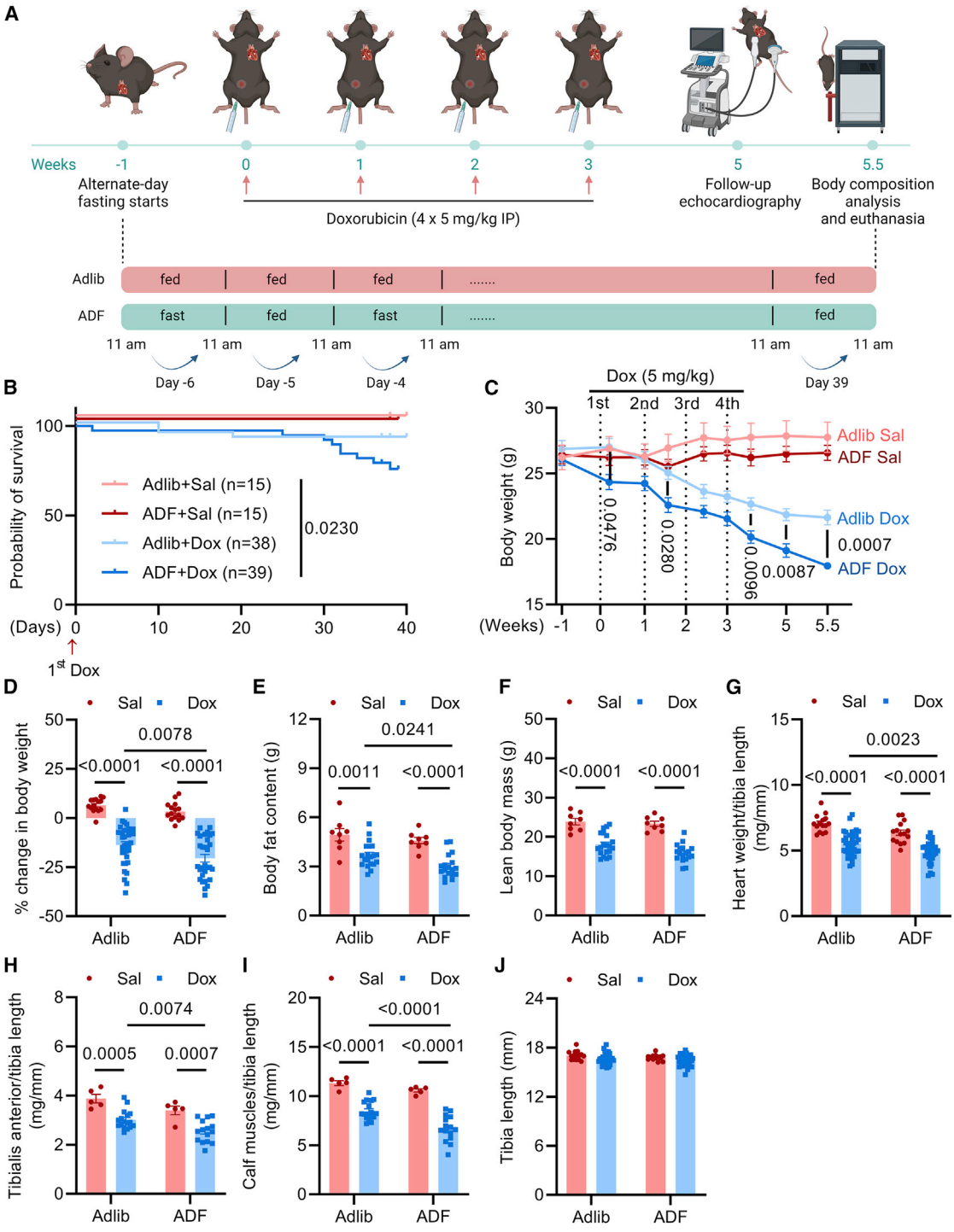

Figure 2. Alternate-day fasting exacerbates doxorubicin-induced mortality and cachexia

(A) Chow-fed C57BL/6 mice (n = 107) were randomized to *ad libitum* or ADF and treated with vehicle or Dox (5 mg/kg i.p. × 4 doses), followed by body composition analysis before euthanasia, as shown in the schematic.

(B) Pooled survival probability in mice from (A) (n = 15–39/group; log-rank test; p value is shown on the graph).

(C) Longitudinal trajectory of body weights throughout the experiment in mice from (A); all measurements are after 24 h of feeding in ADF groups (n = 5–10/group; mixed-effects analysis with Šidák's correction for multiple comparisons; adjusted p values for *ad libitum*-Dox versus ADF-Dox at individual time points are shown on the graph).

(D) Body weight % change in mice from (A) (n = 15–35/group; two-way ANOVA with Šidák's correction for multiple comparisons).

(E) Body fat content in mice from (A) was obtained after 5 weeks on the diet intervention, measured after a feeding day by EchoMRI (n = 8–20/group; two-way ANOVA with Šidák's correction for multiple comparisons).

(legend continued on next page)

Please cite this article in press as: Ozcan et al., Sustained alternate-day fasting potentiates doxorubicin cardiotoxicity, Cell Metabolism (2023), https://doi.org/10.1016/j.cmet.2023.02.006

C57BL/6J and C57BL/6N mice, as diagramed in Figure 2A. Mice were randomized to *ad libitum* feeding or ADF and continued on their respective regimens while receiving Dox (5 mg/kg intraperitoneally [i.p.] weekly). At the time of euthanasia, we performed EchoMRI-based body composition analysis on a fed day. The group that underwent ADF with saline injections did not experience any significant mortality, weight loss, or skeletal muscle loss. Mice randomized to the ADF-Dox group exhibited significantly greater mortality (Figure 2B), progressive body weight loss (Figures 2C and 2D), and loss of fat and lean mass (Figures 2E and 2F). Reductions in lean mass with ADF were non-significant in the overall cohort (Figure 2F; $p = 0.067$), but this was likely due to heterogeneity between male and female mice as well as C57BL/6J and C57BL/6N mice, since ADF provoked significant loss of lean mass in each case when adjusting for gender ($p = 0.006$) or C57 substrain ($p = 0.0003$). Mice that underwent ADF and Dox also exhibited significant reductions in heart and skeletal muscle mass that were normalized to tibia length, compared with Dox-alone mice (Figures 2G–2I), despite similar tibia lengths (Figure 2J). Interestingly, the progressive weight loss began within the first days after Dox in the ADF group (Figure 2C), despite similar food intake at these early time points (Figures S1A–S1C). In particular, while Dox-treated mice exhibited decreased food intake on days they received the drug, they seemed to augment food intake on subsequent days, which the ADF-Dox group did not. Of note, the increased food intake we observed in the Dox group toward the end of the experiment was consistently associated with increased particularization of food and spillage into the cage; hence, we have insufficient evidence to conclude that ADF definitively reduced food intake in the Dox group (Figure S1C).

Echocardiography of C57BL/6 mice receiving Dox consistently demonstrated reduced LV mass/tibia length (Figures 3A and 3B). In the overall cohort, ADF-Dox mice had lower LV mass and ejection fraction than Dox-treated, *ad libitum* mice (Figures 3B and 3C); heart rate, cardiac output, end-diastolic volume, and stroke volume were not significantly different in the *ad libitum* versus ADF groups treated with Dox (Figures 3D–3G). However, because of the increased mortality of the ADF-Dox group (Figure 2B), it is possible that our echo and morphometric data underestimate the degree to which ADF negatively impacted Dox-treated mice.

Although prior reports showed sexual dimorphism in rodents treated with anthracyclines,[16,17] we observed no significant interactions between murine gender and randomization to ADF in C57BL/6J mice treated with Dox (Figures S2A–S2L) regarding body morphometrics, body composition analysis, or cardiotoxicity, with significant, consistent effects of ADF. Male mice in general appeared more sensitive to Dox, and even when female mice deteriorated with ADF combined with Dox, they did so without significant drops in LV ejection fraction (Figure S2H; $p_{interaction}$ for LVEF = 0.09 in females versus males).

C57BL/6J and C57BL/6N mice have been reported to undergo more concentric versus eccentric LV remodeling, respectively, in response to pressure overload stimuli,[18] raising the possibility that the remodeling response may be a variable affecting the interaction between ADF and Dox cardiotoxicity. We therefore performed a study to compare the early response of C57BL/6J versus C57BL/6N mice to Dox (all *ad libitum* fed). Mice underwent echoes at baseline versus 2 weeks post-Dox. C57BL/6J mice lost more weight (Figure S3A; $p_{interaction} < 0.001$) and exhibited a decreased heart rate (Figure S3B; $p_{interaction} < 0.01$) versus C57BL/6N mice. C57BL/6N mice had significantly lower LVEF than C57BL/6J (Figure S3C), whereas C57BL/6J lost significantly greater LV mass, cardiac output, and end-diastolic volume than C57BL/6N mice (Figures S3D–S3F). Despite these differences in remodeling after Dox, we detected no interactions between C57 substrain and ADF in mice that received Dox with consistent, significant effect of ADF, compared with the overall cohort (Figure S4). Overall, our results suggest that the cardiotoxicity of ADF was independent of the murine gender, C57 substrain, or the resultant remodeling response.

Histologic assessment also suggested exacerbation of Dox cardiotoxicity by ADF. The ADF-Dox group exhibited increased myocardial fibrosis (Figures 3H and 3I), reduced cell size (Figures 3J and 3K), and an increased percentage of $TUNEL^+$ nuclei (Figures 3L and 3M). The reduction in cardiac myocyte cross-sectional area with Dox treatment and its exacerbation with ADF (Figure 3J) point to cardiac myocyte atrophy as a mechanism for loss of cardiac mass and LV mass with these interventions (Figures 2G and 3B).

ADF increases myocardial nuclear TFEB, which exacerbates Dox cardiotoxicity

Nuclear protein isolation, isolated on a fed day, from murine myocardial tissue showed increased nuclear TFEB content from mouse hearts that underwent ADF plus Dox (Figures 4A and 4B). Hence the ADF-Dox group, which has increased cardiotoxicity and higher TFEB, parallels what we observed in humans with end-stage failing DC hearts (Figure 1H). Furthermore, ADF plus Dox treatment was associated with significantly reduced mammalian target of rapamycin (mTOR) phosphorylation at Ser2448 and increased MuRF1 (Figures 4C–4F), a known TFEB target in skeletal muscle[14] and mediator of Dox-induced cardiac atrophy,[13] compared with Dox treatment alone.

We next utilized an adeno-associated virus (AAV) TFEB construct (AAV9-CMV-TFEB versus AAV9-CMV-null) that we previously showed had rescued a protein-aggregate

(F) Lean mass in mice from (A) was obtained after 5 weeks on the diet intervention, measured after a feeding day by EchoMRI (n = 8–20/group; two-way ANOVA with Šidák's correction for multiple comparisons).
(G) Heart weight/tibia length in mice from (A) (n = 15–35/group; two-way ANOVA with Šidák's correction for multiple comparisons).
(H) Tibialis anterior muscle weight/tibia length in mice from (A) (n = 5–17/group; two-way ANOVA with Šidák's correction for multiple comparisons).
(I) Calf muscle (gastrocnemius and soleus) weight/tibia length in mice from (A) (n = 5–17/group; two-way ANOVA with Šidák's correction for multiple comparisons).
(J) Tibia length in mice from (A) (n = 15–35/group; two-way ANOVA with Šidák's correction for multiple comparisons, no significant difference).
All mice were sacrificed on a fed day. All data are presented as mean ± SEM and analyzed by GraphPad Prism 9.0. Each dot represents one mouse in (D)–(J). Adjusted p values are shown in (C)–(I).

Please cite this article in press as: Ozcan et al., Sustained alternate-day fasting potentiates doxorubicin cardiotoxicity, Cell Metabolism (2023), https://doi.org/10.1016/j.cmet.2023.02.006

CellPress
OPEN ACCESS

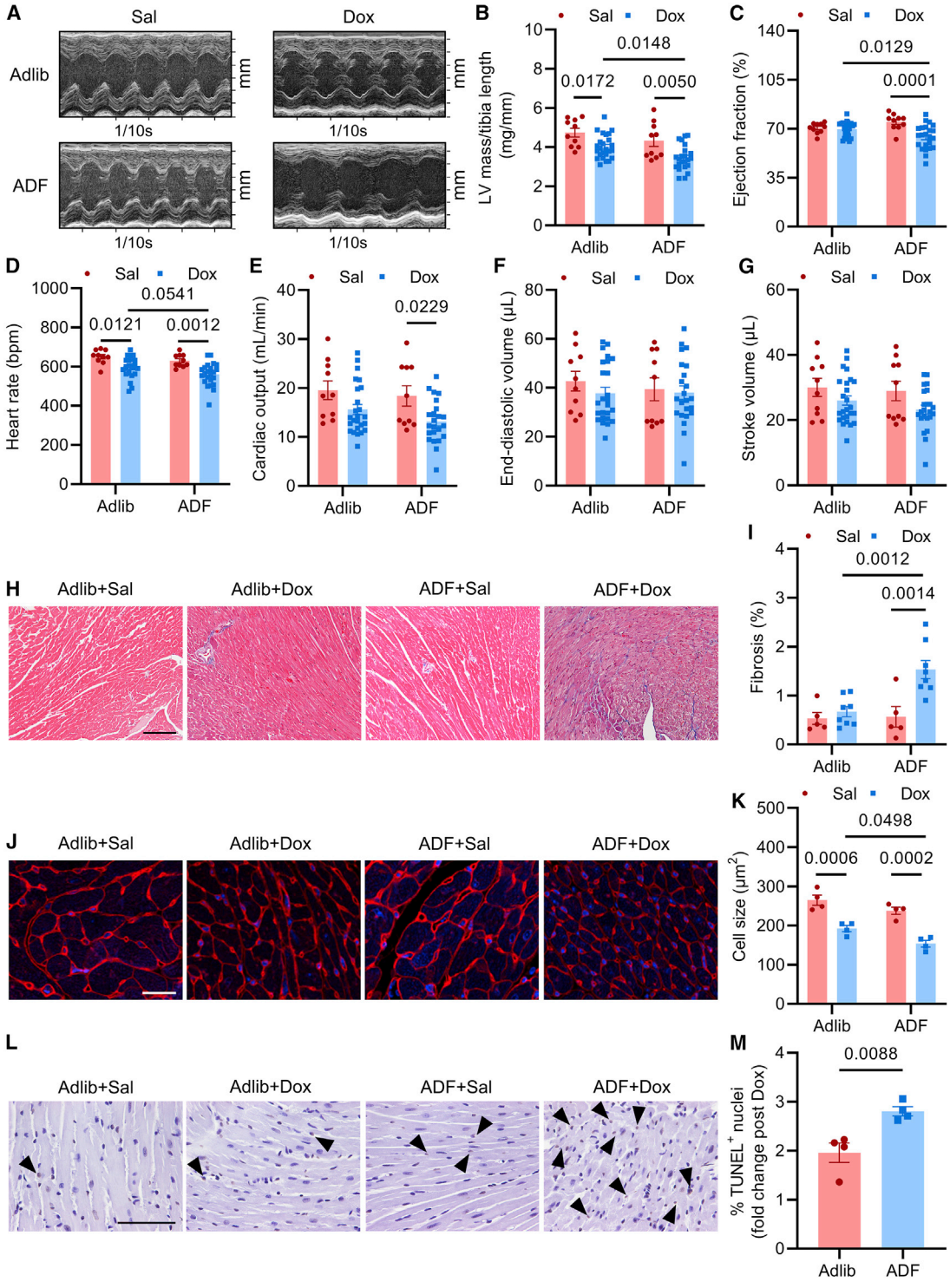

Figure 3. Alternate-day fasting potentiates cardiotoxicity in doxorubicin-treated mice

(A) C57BL/6 mice were randomized to *ad libitum* or ADF and treated with vehicle or Dox (5 mg/kg i.p. × 4 doses) and underwent echocardiography. Representative 2D-directed M-mode echocardiographic images are shown.

(B) Echocardiographic left ventricular (LV) mass/tibia length in mice from (A) (n = 10–25/group; two-way ANOVA with Šidák's correction for multiple comparisons).

(C) Ejection fraction in mice from (A) (n = 10–25/group; two-way ANOVA with Šidák's correction for multiple comparisons).

(D) Heart rate in mice from (A) (n = 10–25/group; two-way ANOVA with Šidák's correction for multiple comparisons).

(E) Cardiac output in mice from (A) (n = 10–25/group; two-way ANOVA with Šidák's correction for multiple comparisons).

(F) End-diastolic volume in mice from (A) (n = 10–25/group; two-way ANOVA, $p > 0.05$).

(legend continued on next page)

Please cite this article in press as: Ozcan et al., Sustained alternate-day fasting potentiates doxorubicin cardiotoxicity, Cell Metabolism (2023), https://doi.org/10.1016/j.cmet.2023.02.006

cardiomyopathy model[2] in the context of saline or Dox. AAV9-CMV-TFEB transduction increased both total and nuclear myocardial TFEB in saline-treated mice (Figures S5A–S5D). After receiving the third dose of Dox, mice that had been injected with AAV9-TFEB rapidly died (Figure 4G). We were able to urgently perform echocardiography in 2 AAV9-CMV-TFEB mice that demonstrated reduced LV mass/tibia length (3.37 mg/mm). Echocardiography of control mice injected with AAV9-CMV-null versus AAV9-CMV-TFEB revealed that in saline-treated animals, TFEB reduced LVEF while simultaneously reducing LV mass (Figures 4H–4L) and qualitatively increased LV fibrosis (Figures S5E and S5F). We next modeled additional mice in the Dox group (not included in the survival study) that we echoed at a pre-morbid time point (12 days post-virus). In these mice, 2 doses of Dox were given prior to the control versus TFEB viral injections to try to ascertain LV structure and function prior to death. AAV9-CMV-TFEB treated with Dox exhibited significantly lower LVEF and increased end-diastolic volume than CMV-null mice (Figures 4M–4Q), with high amounts of fibrosis (Figures S5E and S5F), again consistent with TFEB toxicity.

To determine whether cardiomyocyte-restricted expression of TFEB was also detrimental, we designed a new AAV9 where human HA-TFEB was expressed downstream of the cardiac troponin T (cTNT) promoter (AAV9-cTNT-TFEB versus AAV9-cTNT-GFP controls). Mice in this experiment were given 5 mg/kg Dox (once weekly for 3 weeks) with echocardiography before the first dose, after the second dose, and 1 week after the final dose of Dox (Figure S6A). In this cohort, 1 AAV9-cTNT-TFEB mouse died between echocardiography and euthanasia (Figure S6B), and Dox resulted in similar body weight loss in both groups (Figures S6C and S6D). AAV9-cTNT-TFEB resulted in progressive loss of LV mass (Figure S6E), although LVEF was preserved (Figure S6F). AAV-cTNT-TFEB mice also had a progressive decline in heart rate (Figure S6G), but stroke volume, cardiac output, and end-diastolic volume (Figures S6H–S6J) followed a different pattern and qualitatively increased between the week 2 and week 4 echocardiograms, suggesting that in AAV9-cTNT-TFEB, ventricular dilation may preserve stroke volumes even as LV mass continues to decline.

Given the lower level toxicity of cardiomyocyte-restricted TFEB expression relative to ADF or AAV9-CMV-TFEB transduction, we sought to test whether cardiomyocyte TFEB itself played a role in Dox cardiotoxicity. To do so, we modeled cardiomyocyte-specific TFEB knockouts ($TFEB^{CMKO}$), generated by crossing alpha-myosin heavy-chain Cre (MHC-Cre) mice to previously described $TFEB^{flox}$ mice.[19] Then, 1 week after 2 doses of Dox (5 mg/kg i.p. once weekly), compared with littermate controls, $TFEB^{CMKO}$ mice exhibited less severe body weight loss ($p = 0.054$) and preserved ejection fraction and LV mass (Figures 5A–5D), with statistically significant Dox-induced reductions in these variables occurring only in littermate control mice. Compared with Dox-treated littermate controls, LV mass/tibia length and cell size were significantly higher in $TFEB^{CMKO}$ mice (Figures 5E–5G), while nuclear TFEB (Figures 5H and 5I) and total protein levels of the E3 ubiquitin ligase MuRF1 were lower (Figures 5J and 5K). These results support that deletion of cardiomyocyte TFEB attenuates Dox-mediated cardiac atrophy.

As a further test of the hypothesis that reductions in TFEB prior to treatment with Dox might attenuate the development of cardiotoxicity, we utilized our previously published AAV9-U6-short hairpin construct to knockdown TFEB (AAV9-shTFEB versus AAV9-shScramble control). AAV9-shTFEB previously resulted in ~65% reduction in TFEB protein in the myocardium.[2] Mice underwent baseline echocardiography performed 1 week after viral injections, then repeat echocardiography 1 week after 2 doses of Dox (5 mg/kg i.p.). In this latter experiment, AAV9-mediated TFEB knockdown attenuated reductions in LV mass but not in LVEF (Figures 5L–5N).

Given the significant increase in mortality with systemic TFEB overexpression, we next sought to further define the mechanism by which systemic TFEB overexpression causes mortality and heart failure after Dox. TFEB was recently shown to induce growth differentiation factor 15 (GDF15) in macrophages,[20] and GDF15 is also induced by Dox and associated with Dox cardiotoxicity.[21,22] In *ad libitum* versus ADF mice, plasma GDF15 levels were suppressed on a fed day (Figure 6A), consistent with the increased food intake of ADF mice on fed days. By contrast, Dox blocked ADF-induced GDF15 suppression, as mice randomized to ADF that received Dox had a greater relative induction of GDF15 (Figure 6B). While AAV9-CMV-TFEB transduction stimulated GDF15 in both saline- and Dox-treated mice (Figure 6C), neither TFEB cardiomyocyte-specific knockout nor AAV9-cTNT-TFEB affected circulating GDF15 after Dox (Figures 6D and S6K, respectively). Prior studies of chronic GDF15 administration utilized daily doses of 0.5–1 mg/kg for a total dose of 20–30 mg/kg.[23,24] To determine whether increases in GDF15 were sufficient to induce cardiac atrophy, we performed experiments of low-dose recombinant GDF15 administration (0.3 mg/kg q3 days × 6 doses; Figure 6E). In the first experiment, mice were treated with vehicle (4 mM HCl) or recombinant human GDF15, resulting in significant increases in circulating GDF15 and concomitant reductions in body weight, heart

(G) Stroke volume in mice from (A) (n = 10–25/group; two-way ANOVA with Šidák's correction for multiple comparisons).
(H) Representative images of mid-myocardial sections from mice randomized to *ad libitum* or ADF and treated with vehicle or Dox stained with Masson's trichrome (scale bars, 100 μm).
(I) Blinded quantification of fibrosis from (H) (n = 5–8/group; two-way ANOVA with Šidák's correction for multiple comparisons).
(J) Representative images of mid-myocardial sections from mice randomized to *ad libitum* or ADF and treated with vehicle or Dox stained with wheat germ agglutinin (WGA) (scale bars, 25 μm).
(K) Blinded cell size quantification from (J) (n = 4/group; two-way ANOVA with Šidák's correction for multiple comparisons).
(L) Representative images of TUNEL staining from mid-myocardial sections of mice randomized to *ad libitum* or ADF and treated with vehicle or Dox (scale bars, 50 μm; black triangles show $TUNEL^+$ nuclei).
(M) Blinded quantification of $TUNEL^+$ nuclei from (L) (n = 4/group; Student's t test, p value is shown on the graph).
All echocardiography was performed on a fed day. (B)–(G) were obtained by quantification of blinded echocardiographic assessment (under 2% Avertin, i.p.) of 2D images. All data are presented as mean ± SEM and analyzed by GraphPad Prism 9.0. Adjusted p values are shown in (B)–(G), (I), and (K). Each dot represents one mouse in (B)–(G), (I), (K), and (M).

Please cite this article in press as: Ozcan et al., Sustained alternate-day fasting potentiates doxorubicin cardiotoxicity, Cell Metabolism (2023), https://doi.org/10.1016/j.cmet.2023.02.006

CellPress
OPEN ACCESS

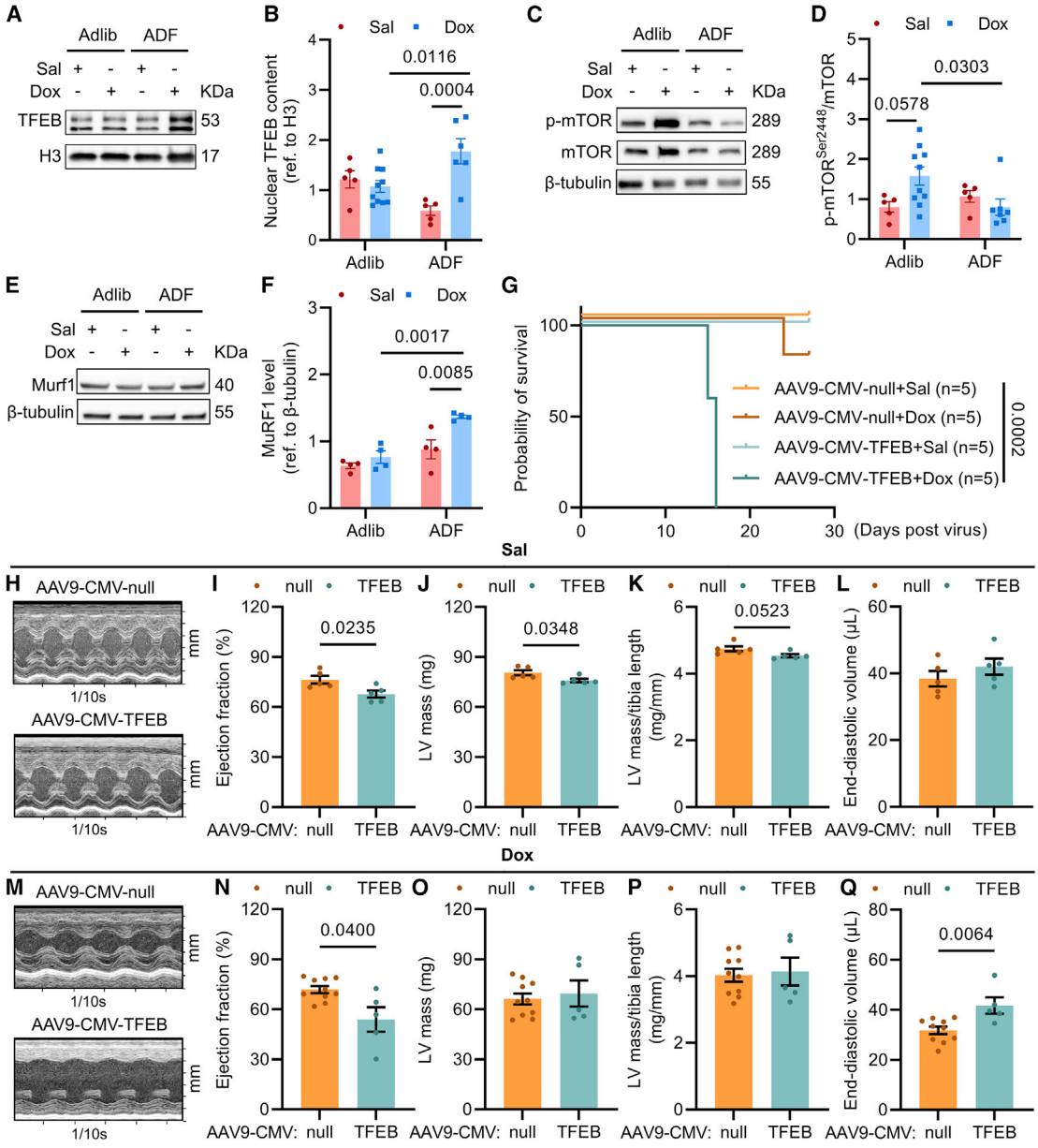

Figure 4. Alternate-day fasting stimulates myocardial TFEB nuclear translocation, which is sufficient to exacerbate mortality in doxorubicin-treated mice

(A) C57BL/6J mice were randomized to *ad libitum* or ADF and were treated with vehicle or Dox (5 mg/kg i.p. × 4 doses) and sacrificed on a fed day. Representative images of immunoblots for TFEB from nuclear myocardial protein lysates are shown; histone H3 serves as a loading control.

(B) Quantification of (A) (n = 5–10/group, two-way ANOVA with Šidák's correction for multiple comparisons).

(C) Myocardial protein lysates were prepared from mice in (A). Representative images of immunoblots for p-mTOR^{Ser2448} and mTOR are shown; β-tubulin serves as a loading control.

(D) Quantification of (C) (n = 5–10/group, two-way ANOVA with Šidák's correction for multiple comparisons).

(E) Myocardial protein lysates were prepared from mice in (A). Representative images of immunoblots for MuRF1 are shown; β-tubulin serves as a loading control.

(F) Quantification of (E) (n = 4/group, two-way ANOVA with Šidák's correction for multiple comparisons).

(G) Survival probability of C57BL/6J mice injected with AAV9-CMV-null or AAV9-CMV-TFEB (3.5 × 10^{11} particles/mouse injected via tail vein) and treated with vehicle or Dox (5 mg/kg i.p. × 4 doses, n = 5/group; log-rank test).

(H) Representative 2D-directed M-mode echocardiographic images 24 days after viral injection of AAV9-CMV-null or AAV9-CMV-TFEB and vehicle control.

(I) Ejection fraction in mice from (H) (n = 5/group, Student's t test).

(J) LV mass in mice from (H) (n = 5/group, Student's t test).

(K) LV mass/tibia length in mice from (H) (n = 5/group, Student's t test).

(L) End-diastolic volume in mice from (H) (n = 5/group, Student's t test, no significant difference).

(legend continued on next page)

Please cite this article in press as: Ozcan et al., Sustained alternate-day fasting potentiates doxorubicin cardiotoxicity, Cell Metabolism (2023), https://doi.org/10.1016/j.cmet.2023.02.006

weight, and LV mass/tibia length (Figures 6F–6I). In a second experiment, mice were treated with Dox (5 mg/kg i.p. × 2 doses) and vehicle or GDF15. GDF15 levels were not significantly higher in mice that received recombinant GDF15 and Dox versus vehicle and Dox (Figure 6J), and GDF15 did not significantly reduce body weight in the presence of Dox (Figure 6K). However, both heart weight and LV mass normalized to tibia length were lower in mice that received both Dox plus GDF15 (Figures 6L and 6M). These experiments suggest that low-dose GDF15 is sufficient to provoke cardiac atrophy, and they provide a potential explanation for the severe toxicity observed with systemic TFEB overexpression.

LV mass and stroke volume correlate in mice treated with Dox and long-term survivors of childhood cancer

Across multiple Dox murine models, we observed that ADF, TFEB, and GDF15 can reduce LV mass prior to the onset of Dox-induced systolic dysfunction. Once there is overt systolic dysfunction, however, TFEB was not associated with decreased LV mass, perhaps due to large increases in end-diastolic volume as mice near death (Figures 4M–4Q). In *ad libitum* and ADF mice given saline or Dox, we observed no correlation of LVEF with stroke volume but consistent linear correlation of LV mass with stroke volume (Figures 7A–7D). These findings were consistent in a cohort of survivors of childhood cancer treated with Dox (Figures 7E and 7F). In these patients, stroke volume was also significantly associated with LV mass index ($r = 0.554$, $p = 0.002$).

DISCUSSION

Utilizing a combination of human heart tissue and murine models, we have found that ADF and TFEB exacerbate Dox-induced cardiotoxicity, in contrast to prior reports.[8,15] Sparked by our finding that human myocardial samples from patients with end-stage DC exhibit increased nuclear TFEB protein abundance, we performed interventions to stimulate TFEB. In 107 mice from two different C57BL/6 substrains and male and female mice, we observed enhanced Dox toxicity with sustained ADF. Importantly, we employed an identical ADF protocol to the one we previously published that was protective in models of diet-induced obesity,[3] ischemia,[5] and protein-aggregate cardiomyopathy.[2]

Although we found that sustained ADF potentiates Dox cardiotoxicity, there are many other modes of IF that may result in different outcomes. In fact, different fasting strategies, including fasting-mimicking diets (FMDs), pioneered by Longo and Brandhorst, have been shown to have lifespan-extending effects in mice (not receiving Dox chemotherapy).[25] These fasting strategies also exert anti-tumor effects and retard tumor growth.[26,27] Because of the number of variables involved in various fasting protocols, our studies do not rule out the possibility that changing the timing of fasting relative to chemotherapy, or a different fasting strategy, may be protective. However, because clinically evident Dox cardiotoxicity (in the absence of aggressive screening) often clinically manifests across longer time periods, our results raise concerns about sustained, prolonged fasting in patients actively receiving Dox chemotherapy.

Mechanistically, both FMD and ADF reduce mTOR pathway activity in mice.[3,4] Although TFEB activation was not confirmed with FMD, we have presently shown that the combination of ADF and Dox reduces myocardial mTOR phosphorylation. Given that mTOR phosphorylates TFEB to regulate its nuclear translocation,[28] export,[29] and hence ability to activate transcription, it is possible that reduced mTOR activity caused increased nuclear, myocardial TFEB in mice. Given the technical limitations with precise food intake measurements in mice, we cannot rule out that for mice that underwent ADF without Dox, increased food intake on fed days caused TFEB suppression, while it is possible that the ADF-Dox mice were not able to keep up in terms of food intake (Figure S1). In saline-treated mice, mice increased their food intake when food was available so that the average food intake was similar. Hence, it is also possible that increased food intake during refeeding allows for TFEB inactivation, although the precise counter-regulatory mechanisms involved were not the focus of the present work.

Fasting is a complex intervention, and the precise mode, timing, and diet composition may affect outcomes. On the one hand, because ADF in the absence of Dox actually reduced circulating GDF15, it is possible that fasting strategies that are undertaken only before Dox administration may be protective against atrophy. The mechanistic basis for GDF15 suppression with ADF alone remains unknown and should be the subject of ongoing study. Furthermore, although our studies suggest a TFEB/MuRF1 pathway, induced by ADF in the setting of Dox, promotes cardiotoxicity, other downstream effects of fasting, including increases in circulating ketones and ketone body metabolism, may improve outcomes in both Dox cardiotoxicity[30] and heart failure.[31,32] Further thorough studies of different fasting interventions will be needed to explore these possibilities.

Our studies contradict prior work suggesting that increasing TFEB nuclear activity attenuates Dox-induced cardiomyocyte cell death[8] and prior observations that ADF is protective in Dox cardiotoxicity.[15] However, we posit that the evidence supporting beneficial effects of sustained ADF and TFEB in the context of Dox cardiotoxicity is not as robust as the data supporting fasting strategies in rodent models of cardiometabolic disease, cancer, and longevity, for example. In fact, studies from Bartlett et al. supporting improved cell survival and other salutary effects of

(M) Representative 2D-directed M-mode echocardiographic images of Dox-treated mice from a second AAV9-CMV-null and TFEB experiment that was modeled due to the extreme mortality in the first experiment (G). Mice underwent echocardiography at early time points after Dox (5 mg/kg i.p. × 3 doses, with 2 doses given prior to viral injection).
(N) Ejection fraction in mice from (M) (n = 5–10/group, Mann-Whitney test).
(O) Echocardiographic LV mass in mice from (M) (n = 5–10/group, Student's t test, no significant difference).
(P) LV mass/tibia length in mice from (M) (n = 5–10/group, Student's t test, no significant difference).
(Q) End-diastolic volume in mice from (M) (n = 5–10/group, Student's t test).
All echocardiography was performed on a fed day. (I)–(L) and (N)–(Q) were obtained by quantification of blinded echocardiographic assessment (under 2% Avertin, i.p.) of 2D images. All data are presented as mean ± SEM and analyzed by GraphPad.

Please cite this article in press as: Ozcan et al., Sustained alternate-day fasting potentiates doxorubicin cardiotoxicity, Cell Metabolism (2023), https://doi.org/10.1016/j.cmet.2023.02.006

CellPress
OPEN ACCESS

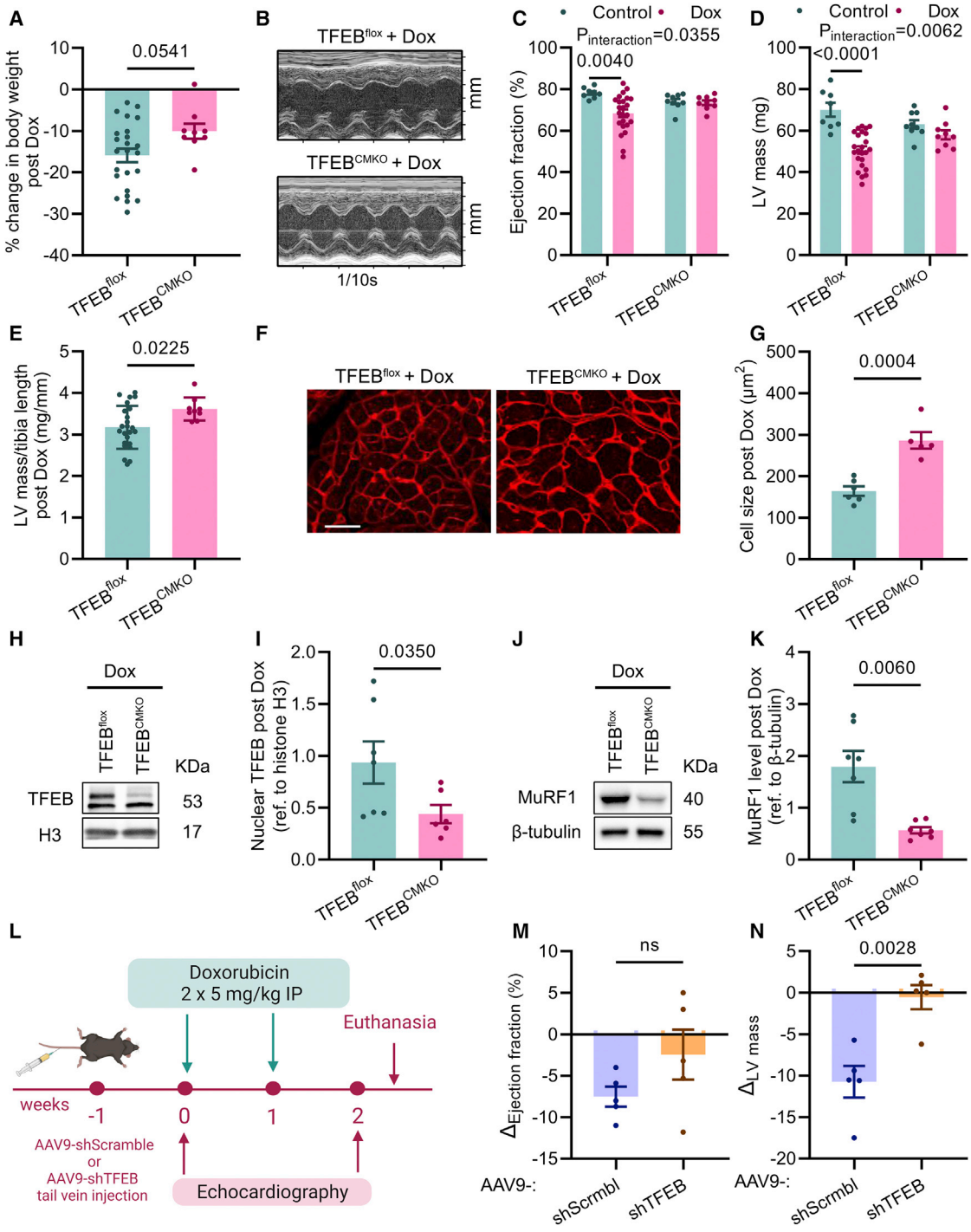

Figure 5. Cardiomyocyte-specific TFEB knockout and AAV9-induced TFEB knockdown alleviated doxorubicin-induced atrophy

(A) % change in body weight in cardiomyocyte-specific TFEB knockout ($TFEB^{CMKO}$) and TFEB flox ($TFEB^{flox}$) littermate mice treated with Dox (5 mg/kg i.p. × 2 doses; n = 9–24/group; Student's t test).

(B) Representative 2D-directed M-mode echocardiographic images in mice from (A).

(C) Ejection fraction in $TFEB^{CMKO}$ and $TFEB^{flox}$ littermate mice treated with vehicle (control) or Dox (5 mg/kg i.p. × 2 doses; n = 8–24/group; two-way ANOVA with Šidák's correction for multiple comparisons).

(D) Echocardiographic left ventricular (LV) mass in mice from (C) (n = 8–24/group; two-way ANOVA with Šidák's correction for multiple comparisons).

(E) Echocardiographic LV mass/tibia length in Dox-treated mice from (C) (n = 9–24/group; Student's t test).

(F) Representative images of mid-myocardial sections from Dox-treated mice in (C), stained with wheat germ agglutinin (WGA) (scale bars, 25 μm).

(G) Blinded cell size quantification from (F) (n = 5–6/group; Student's t test).

(legend continued on next page)

Please cite this article in press as: Ozcan et al., Sustained alternate-day fasting potentiates doxorubicin cardiotoxicity, Cell Metabolism (2023), https://doi.org/10.1016/j.cmet.2023.02.006

TFEB were based primarily on *in vitro* (cellular) models, while our present studies utilize both physiological and viral TFEB stimuli in much larger *in vivo* experiments.

Bartlett et al. also found that Dox reduces TFEB acutely, but we show that increases in TFEB exacerbate Dox cardiotoxicity (Figures 4 and S5). This is concordant with our human data, whereby patients who have acquired heart failure, in most cases years after Dox exposure, have high, not low, TFEB nuclear protein abundance in the myocardium (Figure 1). In our murine studies, the physiological stimulus of ADF resulted in increased nuclear TFEB, increased myocardial fibrosis, and cell death when added to Dox treatment. In the only other prior study of sustained ADF and ADF cardiotoxicity, a methodology similar to ours (ADF followed by Dox administration by i.p. injection) was employed; however, group sizes were small (typically n = 3) and neither survival, echocardiographic, nor morphometric data were provided.[15] Our data are also supported by those of Li et al., who originally found that Dox impairs lysosomal acidification but also reported that mice with autophagic impairment due to heterozygous deletion of Beclin-1 were protected from Dox cardiotoxicity.[1]

Another central finding of our work is that ADF and systemic TFEB activation stimulated weight loss and mortality after Dox, while cardiomyocyte-specific TFEB overexpression did not. One possible explanation for this is that TFEB in non-cardiomyocytes stimulates GDF15,[20] which has previously been shown to be induced by Dox[21] and has been associated with Dox cardiotoxicity.[22] GDF15 is known to play a causal role in cachexia in murine models, as GDF15 antagonism reversed cancer cachexia in mice.[33] We found that systemic TFEB overexpression resulted in large increases in circulating GDF15 and that even low-dose GDF15 was sufficient to potentiate cardiac atrophy, either in the presence or absence of Dox. While ADF by itself suppressed GDF15, mice exposed to Dox plus ADF failed to suppress GDF15. The fact that ADF suppresses GDF15 on a fed day is concordant with the increased food intake on that day in mice randomized to ADF. One possibility is that augmentation of food intake is required for TFEB and GDF15 suppression, and mice given Dox are unable to sufficiently augment food intake on fed days. Indeed, consistent with reductions in GDF15 with ADF alone, ADF without Dox does not cause weight loss, cachexia, or cardiac atrophy in mice. It is hence plausible that failure to suppress GDF15 in the context of sustained fasting leads to progressive cachexia in mice.

As opposed to systemic overexpression, cardiomyocyte TFEB did not play a role in GDF15 increases. However, our studies show that cardiomyocyte TFEB was necessary for Dox cardiotoxicity, possibly through MuRF1. Cardiomyocyte-restricted overexpression of TFEB was sufficient to enhance LV mass loss, while cardiomyocyte-specific knockout of TFEB attenuated Dox-induced reductions in LV mass. Compared with littermate controls, cardiomyocyte-specific knockout of TFEB was also associated with higher cell size and lower MuRF1 protein levels in Dox-treated mice. Hence, cardiomyocyte TFEB may potentiate cardiac atrophy through MuRF1, whereas non-myocyte TFEB may potentiate cardiac atrophy through GDF15. Both MuRF1 and GDF15 therefore likely independently contribute to the cardiac atrophy observed in Dox models. Whereas our data support a cell-autonomous role for TFEB in Dox-induced cardiomyocyte atrophy, mice transduced with CMV-TFEB and treated with Dox exhibited more severe cardiotoxicity, reduced LVEF, increased fibrosis, and mortality.

Further human relevance of these findings is underscored by the observation that in mice that underwent either *ad libitum* feeding or ADF, we observed a significant, positive correlation between LV mass and stroke volume. We observe similar correlations of LV mass and stroke volume in childhood survivors of pediatric cancers. These findings may potentially explain prior observations that loss of LV mass is associated with both mortality[34] and decreased quality of life in patients treated with anthracyclines.[12] Either ADF or sustained activation of TFEB can cause progressive loss of LV mass, even in the setting of LV dilatation, which points to cardiac atrophy. Our data emphasize the importance of pathways regulating LV mass and cachexia in the setting of Dox chemotherapy and suggest increased clinical vigilance of the relationship between caloric intake and chemotherapy-associated cachexia and cardiotoxicity.

Limitations of study

Both our human and murine data should be interpreted in the context of study limitations. First, our observation of increased nuclear TFEB in human heart tissue from patients who have received Dox is based on a limited number of Dox samples (n = 11), although this is one of the larger sample sizes we are aware of in this condition. The human observations are correlative in nature but unlikely to represent a general stress response, as heart tissue from patients with NICM, also obtained at time of cardiac transplantation, did not show increased nuclear TFEB. Despite large variations in nuclear TFEB levels in patients with DC, heart tissue from patients with DC exhibited higher nuclear TFEB content than donors, even when the four samples with the highest TFEB levels were excluded from the DC group

(H) Nuclear myocardial protein lysates were prepared from mice in (A). Representative images of immunoblots for TFEB are shown; histone H3 serves as a loading control.
(I) Quantification of (H) (n = 6–7/group; Mann-Whitney test).
(J) Myocardial protein lysates were prepared from mice in (A). Representative images of immunoblots for MuRF1 are shown; β-tubulin serves as a loading control.
(K) Quantification of (H) (n = 7/group; Student's t test with Welch's correction).
(L) C57BL/6J mice were injected with AAV9-shScramble or AAV9-shTFEB (3.5×10^{11} particles/mouse injected via tail vein) and treated with doxorubicin (5 mg/kg i.p. × 2 doses; n = 5/group) with echocardiography baseline at 1 week after post-virus injections and follow-up at 1 week after second doxorubicin treatment, as shown in the schematic.
(M) Absolute change of ejection fraction from baseline in each mouse from (J) at week 2 (Student's t test).
(N) Absolute change of LV mass from baseline in each mouse from (J) at week 2 (Student's t test).
All echocardiography was performed on a fed day. (C)–(E), (M), and (N) were obtained by quantification of blinded echocardiographic assessment (under 2% Avertin, i.p.) of 2D images. All data are presented as mean ± SEM and analyzed by GraphPad Prism 9.0. Adjusted p values are shown in (C) and (D). p values are shown in (A), (E), (G), (I), (K), (M), and (N). Each dot represents one mouse in (A), (C)–(E), (G), (I), (K), (M), and (N).

Please cite this article in press as: Ozcan et al., Sustained alternate-day fasting potentiates doxorubicin cardiotoxicity, Cell Metabolism (2023), https://doi.org/10.1016/j.cmet.2023.02.006

CellPress
OPEN ACCESS

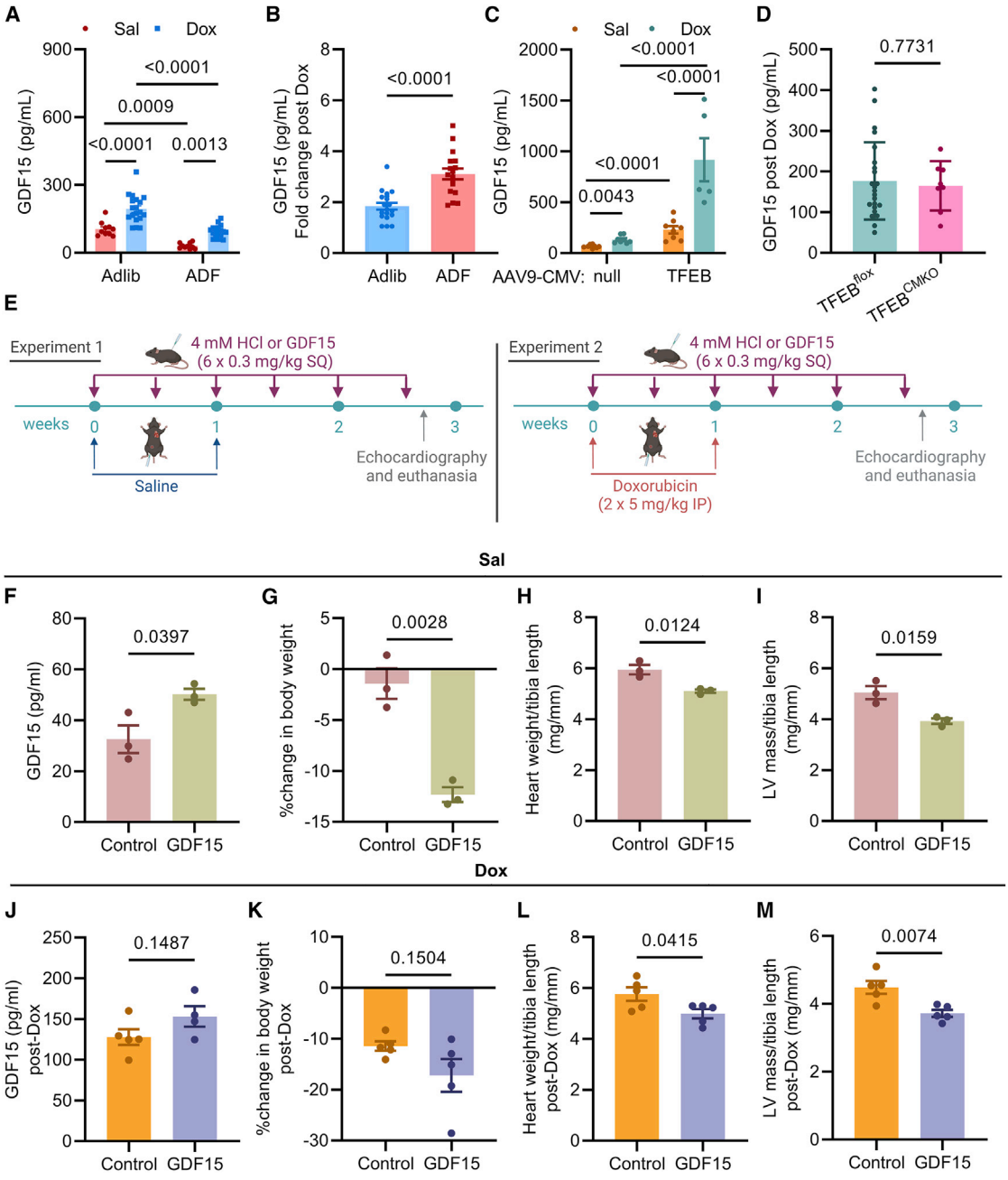

Figure 6. TFEB increases GDF15, which is sufficient to reduce LV mass in mice

(A) GDF15 plasma concentrations in C57BL/6J mice randomized to *ad libitum* or ADF and treated with vehicle or Dox (5 mg/kg i.p. × 4 doses) (n = 10–19/group; two-way ANOVA with Šidák's correction for multiple comparisons).

(B) GDF15 fold change in mice from (A) (n = 10–19/group; Student's t test).

(C) GDF15 plasma concentrations in mice from AAV9-CMV-null versus AAV9-CMV-TFEB viral transduction experiments from Figures 4H–4Q (n = 5–8/group; two-way ANOVA with Šidák's correction for multiple comparisons were used to analyze log transformed data, since residuals violated normality assumptions).

(D) Plasma GDF15 from cardiomyocyte-specific TFEB knockout ($TFEB^{CMKO}$) and TFEB flox ($TFEB^{flox}$) littermate mice treated with Dox (n = 8–23/group; Student's t test).

(E) In one experiment, chow-fed C57BL/6J mice were randomized to receive saline injection plus vehicle control (4 mM HCl) or saline injection plus GDF15 (0.3 mg/kg × 6 doses SQ) (n = 3/group). In a second experiment, mice received Dox (5 mg/kg i.p.) plus control (4 mM HCl) or Dox plus GDF15 (0.3 mg/kg SQ × 6 doses) (n = 5/group), as shown in the schematic.

(F) Plasma GDF15 levels in saline-treated mice from (E) (n = 3/group; Student's t test).

(G) % change in body weight in saline-treated mice from (E) (n = 3/group; Student's t test).

(H) Heart weight/tibia length in saline-treated mice from (E) (n = 3/group; Student's t test).

(I) Echocardiographic left ventricular (LV) mass/tibia length in saline-treated mice from (E) (n = 3/group; Student's t test).

(legend continued on next page)

Please cite this article in press as: Ozcan et al., Sustained alternate-day fasting potentiates doxorubicin cardiotoxicity, Cell Metabolism (2023), https://doi.org/10.1016/j.cmet.2023.02.006

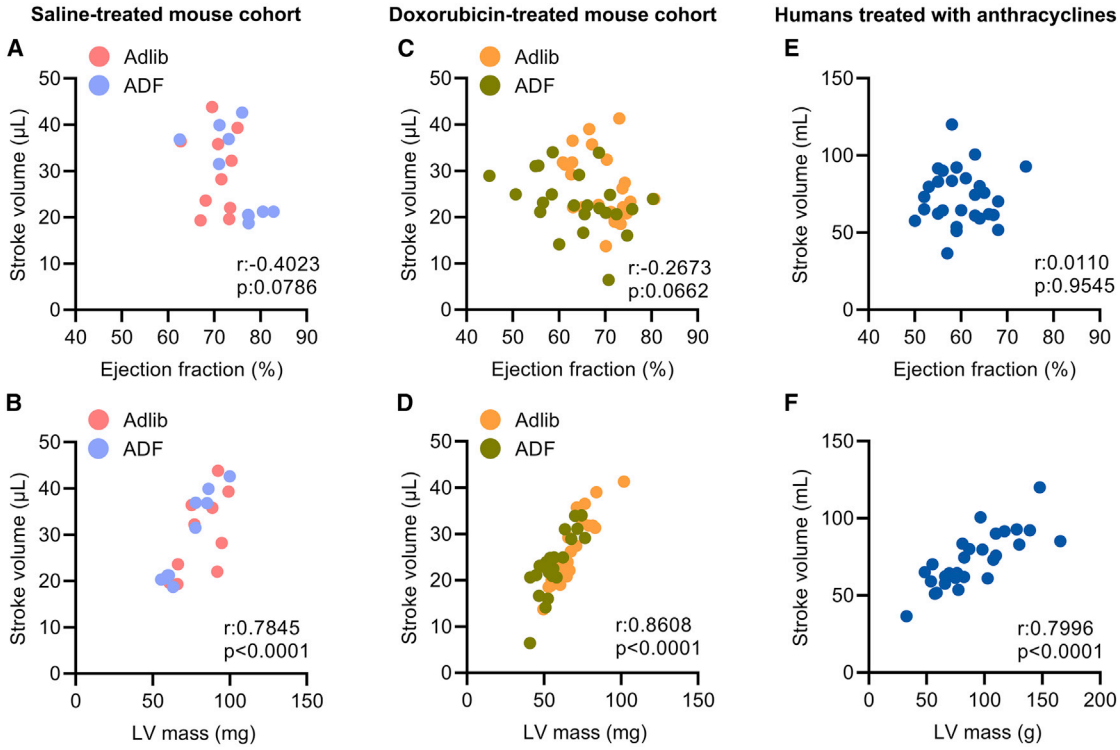

Figure 7. LV mass, but not LV ejection fraction, correlates with stroke volume in mice and survivors of childhood cancers treated with doxorubicin

(A) Correlation of stroke volume versus LV ejection fraction in C57BL/6 saline-treated mice randomized to *ad libitum* or ADF with echocardiographic data (n = 20, Pearson correlation coefficient [r] and p value are shown on the graph).

(B) Correlation of stroke volume versus LV mass in mice from (A) (n = 20, Pearson correlation coefficient [r] and p value are shown on the graph).

(C) Correlation of stroke volume versus LV ejection fraction in C57BL/6 doxorubicin-treated mice randomized to *ad libitum* or ADF with echocardiographic data (n = 48, Pearson correlation coefficient [r] and p value are shown on the graph).

(D) Correlation of stroke volume versus LV mass in mice from (C) (n = 48, Pearson correlation coefficient [r] and p value are shown on the graph).

(E) Correlation of stroke volume versus LV ejection fraction in survivors of childhood cancers treated with anthracyclines (n = 29, Pearson correlation coefficient [r] and p value are shown on the graph).

(F) Correlation of stroke volume versus LV mass in humans from (E) (n = 29, Pearson correlation coefficient [r] and p value are shown on the graph).

Mouse echocardiography was performed on a fed day. (A)–(D) were obtained by quantification of blinded echocardiographic assessment (under 2% Avertin, i.p.) of 2D images. (E) and (F) were obtained by cardiac MRI and calculated from EKG-gated steady-state free precession (SSFP). All data were analyzed by GraphPad Prism 9.0. Each dot represents one mouse or one person.

(p = 0.0339). However, since patients were treated with Dox years before sample procurement at transplant, many possible additional confounders could be contributing to increased nuclear TFEB levels. Whether TFEB levels are altered in heart tissue from patients with Dox exposure more generally would require a sample of donors without heart failure who were previously exposed to Dox.

With respect to our murine studies, although ADF decreased LVEF in Dox-treated mice, LVEF changes were typically clinically modest. In general, murine models of Dox administration alone do not model the end-stage DC observed in humans but are more likely indicative of early Dox cardiotoxicity. Although sustained fasting exacerbated Dox cardiotoxicity in mice, mice may be dying of systemic effects, and we cannot be certain of the mode of death. Our study focused on ADF as a fasting strategy based on both our own prior studies and current data that ADF increases TFEB activity in disease models. While we showed that TFEB was necessary and sufficient to worsen Dox cardiotoxicity, we did not test other potential effects of fasting or whether other fasting strategies also provoke Dox

(J) Plasma GDF15 levels in Dox-treated mice from (E) (n = 4–5/group; Student's t test).

(K) % change in body weight in Dox-treated mice from (E) (n = 5/group; Student's t test with Welch's correction).

(L) Heart weight/tibia length in Dox-treated mice from (E) (n = 5/group; Student's t test).

(M) Echocardiographic left ventricular (LV) mass/tibia length in Dox-treated mice from (E) (n = 5/group; Student's t test).

All echocardiography was performed on a fed day. (I) and (M) were obtained by quantification of blinded echocardiographic assessment (under 2% Avertin, i.p.) of 2D images. All data are presented as mean ± SEM and analyzed by GraphPad Prism 9.0. Adjusted p values are shown on (A) and (C). p values are shown on (B), (D), and (F)–(M). Each dot represents one mouse in (A)–(D) and (F)–(M).

cardiotoxicity. Because sustained ADF in the absence of Dox suppressed GDF15, it is clear that there are many possibilities for how differing fasting strategies may result in differing outcomes. The mechanism by which ADF reduces GDF15 is beyond the scope of the present study, but this study may explain why sustained ADF, on its own, did not cause cachexia or death in mice.

STAR★METHODS

Detailed methods are provided in the online version of this paper and include the following:

- KEY RESOURCES TABLE
- RESOURCE AVAILABILITY
  - Lead contact
  - Materials availability
  - Data and code availability
- EXPERIMENTAL MODEL AND SUBJECT DETAILS
  - Heart tissue cohort
  - Cardiac MRI cohort of pediatric cancer survivors
  - Study approval
  - Rodent studies
- METHOD DETAILS
  - Reagents
  - Doxorubicin cardiotoxicity studies
  - Adeno-associated virus experiments
  - Recombinant human GDF15 experiments
  - Cardiomyocyte-specific TFEB knockout experiments
  - Assessment of body weight and body composition
  - Enzyme-linked immunosorbent assay (ELISA)
  - Histologic analyses
  - Cytoplasmic and nuclear protein extraction
  - Total protein extraction
  - Western blot analysis
- QUANTIFICATION AND STATISTICAL ANALYSIS

SUPPLEMENTAL INFORMATION

Supplemental information can be found online at https://doi.org/10.1016/j.cmet.2023.02.006.

ACKNOWLEDGMENTS

A.J. was supported by K08HL138262 and 1R01HL155344 from the NHLBI; by the Children's Discovery Institute of Washington University (MC-FR-2020-919) and St. Louis Children's Hospital, as well as the Diabetes Research Center at Washington University in St. Louis of the National Institutes of Health under award number P30DK020579; and by NIH grant P30DK056341 (Nutrition Obesity Research Center). Z.G. was supported by the American Heart Association Postdoctoral Fellowship (898679). A.A. was supported by K08HL145019. A. Diwan was supported by grants from the Department of Veterans Affairs (I01BX004235) and the National Institutes of Health (HL107594, HL143431, and NS094692). C.B. was supported by R01HL147884. We acknowledge support from the Advanced Imaging and Tissue Analysis Core of the Digestive Disease Research Core Center (DDRCC NIH P30DK052574) at Washington University School of Medicine. Funding for human cardiac MRI data was provided by the Children's Discovery Institute of Washington University and St. Louis Children's Hospital, grant number MC-II-2020-893. This work was supported by the Hope Center Viral Vectors Core at Washington University School of Medicine.

AUTHOR CONTRIBUTIONS

M.O. and Z.G. designed and performed the experiments, analyzed the data, interpreted the results, and wrote the article. A.J. designed the experiments, interpreted the results, and wrote the article. A. Diwan, C.B., A.A., J. Schilling, and B.R. interpreted the results and wrote the article. C.V.R., A. Diab, and A.P. performed the experiments and interpreted the results. D.R., A.L., D.H., and A.K. performed the experiments. K.B.M., M.K., J.Z., R.J.H., and P.K.W. provided critical materials. J. Szymanski gave consultation about biostatistics and wrote the statistical methods.

DECLARATION OF INTERESTS

A.J. has a pending patent for fusion protein nanodiscs for the treatment of heart failure and eye disease, is a member of the scientific advisory board of Mobius Scientific, and receives research funding from AstraZeneca, unrelated to the studies in this manuscript. M.K. receives consulting fees/honoraria from AstraZeneca, Amgen, Sanofi-Aventis, Boehringer Ingelheim, Glytec, Merck, Janssen Pharmaceuticals, Novartis, Applied Therapeutics, Bayer Healthcare Pharmaceuticals, Eli Lilly and Company, and Vifor Pharma and research grants from AstraZeneca and Boehringer Ingelheim. A. Diwan reports consulting for clinical trials with Clario (previously ERT/Biomedical systems) and serves on the scientific advisory board for Dewpoint Therapeutics, which are not relevant to the current study.

Received: January 4, 2022
Revised: November 24, 2022
Accepted: February 7, 2023
Published: March 2, 2023

REFERENCES

1. Li, D.L., Wang, Z.V., Ding, G., Tan, W., Luo, X., Criollo, A., Xie, M., Jiang, N., May, H., Kyrychenko, V., et al. (2016). Doxorubicin blocks cardiomyocyte autophagic flux by inhibiting lysosome acidification. Circulation *133*, 1668–1687. https://doi.org/10.1161/CIRCULATIONAHA.115.017443.
2. Ma, X., Mani, K., Liu, H., Kovacs, A., Murphy, J.T., Foroughi, L., French, B.A., Weinheimer, C.J., Kraja, A., Benjamin, I.J., et al. (2019). Transcription factor EB activation rescues advanced alphaB-crystallin mutation-induced cardiomyopathy by normalizing desmin localization. J. Am. Heart Assoc. *8*, e010866. https://doi.org/10.1161/JAHA.118.010866.
3. Liu, H., Javaheri, A., Godar, R.J., Murphy, J., Ma, X., Rohatgi, N., Mahadevan, J., Hyrc, K., Saftig, P., Marshall, C., et al. (2017). Intermittent fasting preserves beta-cell mass in obesity-induced diabetes via the autophagy-lysosome pathway. Autophagy *13*, 1952–1968. https://doi.org/10.1080/15548627.2017.1368596.
4. Cheng, C.W., Villani, V., Buono, R., Wei, M., Kumar, S., Yilmaz, O.H., Cohen, P., Sneddon, J.B., Perin, L., and Longo, V.D. (2017). Fasting-mimicking diet promotes Ngn3-driven beta-cell regeneration to reverse diabetes. Cell *168*, 775–788.e12. https://doi.org/10.1016/j.cell.2017.01.040.
5. Godar, R.J., Ma, X., Liu, H., Murphy, J.T., Weinheimer, C.J., Kovacs, A., Crosby, S.D., Saftig, P., and Diwan, A. (2015). Repetitive stimulation of autophagy-lysosome machinery by intermittent fasting preconditions the myocardium to ischemia-reperfusion injury. Autophagy *11*, 1537–1560. https://doi.org/10.1080/15548627.2015.1063768.
6. Mani, K., Javaheri, A., and Diwan, A. (2018). Lysosomes mediate benefits of intermittent fasting in cardiometabolic disease: the janitor is the undercover boss. Compr. Physiol. *8*, 1639–1667. https://doi.org/10.1002/cphy.c180005.
7. Guo, Z., Valenzuela Ripoll, C., Picataggi, A., Rawnsley, D.R., Ozcan, M., Chirinos, J.A., Chendamarai, E., Girardi, A., Riehl, T., Evie, H., et al. (2023). Apolipoprotein M attenuates anthracycline cardiotoxicity and lysosomal injury. J. Am. Coll. Cardiol. Basic Trans. Science. https://doi.org/10.1016/j.jacbts.2022.09.010.

8. Bartlett, J.J., Trivedi, P.C., Yeung, P., Kienesberger, P.C., and Pulinilkunnil, T. (2016). Doxorubicin impairs cardiomyocyte viability by suppressing transcription factor EB expression and disrupting autophagy. Biochem. J. *473*, 3769–3789. https://doi.org/10.1042/BCJ20160385.

9. Lowe, D.A., Wu, N., Rohdin-Bibby, L., Moore, A.H., Kelly, N., Liu, Y.E., Philip, E., Vittinghoff, E., Heymsfield, S.B., Olgin, J.E., et al. (2020). Effects of time-restricted eating on weight loss and other metabolic parameters in women and men with overweight and obesity: the TREAT randomized clinical trial. JAMA Intern. Med. *180*, 1491–1499. https://doi.org/10.1001/jamainternmed.2020.4153.

10. Roman, Y.M., Dominguez, M.C., Easow, T.M., Pasupuleti, V., White, C.M., and Hernandez, A.V. (2019). Effects of intermittent versus continuous dieting on weight and body composition in obese and overweight people: a systematic review and meta-analysis of randomized controlled trials. Int. J. Obes. (Lond) *43*, 2017–2027. https://doi.org/10.1038/s41366-018-0204-0.

11. Alhamdan, B.A., Garcia-Alvarez, A., Alzahrnai, A.H., Karanxha, J., Stretchberry, D.R., Contrera, K.J., Utria, A.F., and Cheskin, L.J. (2016). Alternate-day versus daily energy restriction diets: which is more effective for weight loss? A systematic review and meta-analysis. Obes. Sci. Pract. *2*, 293–302. https://doi.org/10.1002/osp4.52.

12. Jordan, J.H., Castellino, S.M., Meléndez, G.C., Klepin, H.D., Ellis, L.R., Lamar, Z., Vasu, S., Kitzman, D.W., Ntim, W.O., Brubaker, P.H., et al. (2018). Left ventricular mass change after anthracycline chemotherapy. Circ. Heart Fail. *11*, e004560. https://doi.org/10.1161/CIRCHEARTFAILURE.117.004560.

13. Willis, M.S., Parry, T.L., Brown, D.I., Mota, R.I., Huang, W., Beak, J.Y., Sola, M., Zhou, C., Hicks, S.T., Caughey, M.C., et al. (2019). Doxorubicin exposure causes subacute cardiac atrophy dependent on the striated muscle-specific ubiquitin ligase MuRF1. Circ. Heart Fail. *12*, e005234. https://doi.org/10.1161/CIRCHEARTFAILURE.118.005234.

14. Du Bois, P., Pablo Tortola, C., Lodka, D., Kny, M., Schmidt, F., Song, K., Schmidt, S., Bassel-Duby, R., Olson, E.N., and Fielitz, J. (2015). Angiotensin II induces skeletal muscle atrophy by activating TFEB-mediated MuRF1 expression. Circ. Res. *117*, 424–436. https://doi.org/10.1161/CIRCRESAHA.114.305393.

15. An, L., Hu, X.W., Zhang, S., Hu, X., Song, Z., Naz, A., Zi, Z., Wu, J., Li, C., Zou, Y., et al. (2017). UVRAG deficiency exacerbates doxorubicin-induced cardiotoxicity. Sci. Rep. *7*, 43251. https://doi.org/10.1038/srep43251.

16. Grant, M.K.O., Seelig, D.M., Sharkey, L.C., Choi, W.S.V., Abdelgawad, I.Y., and Zordoky, B.N. (2019). Sexual dimorphism of acute doxorubicin-induced nephrotoxicity in C57BL/6 mice. PLoS One *14*, e0212486. https://doi.org/10.1371/journal.pone.0212486.

17. Moulin, M., Piquereau, J., Mateo, P., Fortin, D., Rucker-Martin, C., Gressette, M., Lefebvre, F., Gresikova, M., Solgadi, A., Veksler, V., et al. (2015). Sexual dimorphism of doxorubicin-mediated cardiotoxicity: potential role of energy metabolism remodeling. Circ. Heart Fail. *8*, 98–108. https://doi.org/10.1161/CIRCHEARTFAILURE.114.001180.

18. Garcia-Menendez, L., Karamanlidis, G., Kolwicz, S., and Tian, R. (2013). Substrain specific response to cardiac pressure overload in C57BL/6 mice. Am. J. Physiol. Heart Circ. Physiol. *305*, H397–H402. https://doi.org/10.1152/ajpheart.00088.2013.

19. Trivedi, P.C., Bartlett, J.J., Mercer, A., Slade, L., Surette, M., Ballabio, A., Flibotte, S., Hussein, B., Rodrigues, B., Kienesberger, P.C., and Pulinilkunnil, T. (2020). Loss of function of transcription factor EB remodels lipid metabolism and cell death pathways in the cardiomyocyte. Biochim. Biophys. Acta Mol. Basis Dis. *1866*, 165832. https://doi.org/10.1016/j.bbadis.2020.165832.

20. Kim, J., Kim, S.H., Kang, H., Lee, S., Park, S.Y., Cho, Y., Lim, Y.M., Ahn, J.W., Kim, Y.H., Chung, S., et al. (2021). TFEB-GDF15 axis protects against obesity and insulin resistance as a lysosomal stress response. Nat. Metab. *3*, 410–427. https://doi.org/10.1038/s42255-021-00368-w.

21. Kaya, F., Arslan, D., Vatansev, H., Kose, D., Cimen, D., Akyurek, F., Oran, B., and Koksal, Y. (2016). Growth-differentiation factor-15 and tissue Doppler imaging in detection of anthracycline-induced cardiomyopathy during therapy of childhood cancers. J. Pediatr. Hematol. Oncol. *38*, e107–e112. https://doi.org/10.1097/MPH.0000000000000491.

22. Putt, M., Hahn, V.S., Januzzi, J.L., Sawaya, H., Sebag, I.A., Plana, J.C., Picard, M.H., Carver, J.R., Halpern, E.F., Kuter, I., et al. (2015). Longitudinal changes in multiple biomarkers are associated with cardiotoxicity in breast cancer patients treated with doxorubicin, taxanes, and trastuzumab. Clin. Chem. *61*, 1164–1172. https://doi.org/10.1373/clinchem.2015.241232.

23. Tsai, V.W., Zhang, H.P., Manandhar, R., Lee-Ng, K.K.M., Lebhar, H., Marquis, C.P., Husaini, Y., Sainsbury, A., Brown, D.A., and Breit, S.N. (2018). Treatment with the TGF-b superfamily cytokine MIC-1/GDF15 reduces the adiposity and corrects the metabolic dysfunction of mice with diet-induced obesity. Int. J. Obes. (Lond) *42*, 561–571. https://doi.org/10.1038/ijo.2017.258.

24. Xu, J., Kimball, T.R., Lorenz, J.N., Brown, D.A., Bauskin, A.R., Klevitsky, R., Hewett, T.E., Breit, S.N., and Molkentin, J.D. (2006). GDF15/MIC-1 functions as a protective and antihypertrophic factor released from the myocardium in association with SMAD protein activation. Circ. Res. *98*, 342–350. https://doi.org/10.1161/01.RES.0000202804.84885.d0.

25. Brandhorst, S., Choi, I.Y., Wei, M., Cheng, C.W., Sedrakyan, S., Navarrete, G., Dubeau, L., Yap, L.P., Park, R., Vinciguerra, M., et al. (2015). A periodic diet that mimics fasting promotes multi-system regeneration, enhanced cognitive performance, and healthspan. Cell Metab. *22*, 86–99. https://doi.org/10.1016/j.cmet.2015.05.012.

26. Brandhorst, S. (2021). Fasting and fasting-mimicking diets for chemotherapy augmentation. GeroScience *43*, 1201–1216. https://doi.org/10.1007/s11357-020-00317-7.

27. Lee, C., Raffaghello, L., Brandhorst, S., Safdie, F.M., Bianchi, G., Martin-Montalvo, A., Pistoia, V., Wei, M., Hwang, S., Merlino, A., et al. (2012). Fasting cycles retard growth of tumors and sensitize a range of cancer cell types to chemotherapy. Sci. Transl. Med. *4*, 124ra27. https://doi.org/10.1126/scitranslmed.3003293.

28. Roczniak-Ferguson, A., Petit, C.S., Froehlich, F., Qian, S., Ky, J., Angarola, B., Walther, T.C., and Ferguson, S.M. (2012). The transcription factor TFEB links mTORC1 signaling to transcriptional control of lysosome homeostasis. Sci. Signal. *5*, ra42. https://doi.org/10.1126/scisignal.2002790.

29. Napolitano, G., Esposito, A., Choi, H., Matarese, M., Benedetti, V., Di Malta, C., Monfregola, J., Medina, D.L., Lippincott-Schwartz, J., and Ballabio, A. (2018). mTOR-dependent phosphorylation controls TFEB nuclear export. Nat. Commun. *9*, 3312. https://doi.org/10.1038/s41467-018-05862-6.

30. Liu, Y., Wei, X., Wu, M., Xu, J., Xu, B., and Kang, L. (2020). Cardioprotective roles of beta-hydroxybutyrate against doxorubicin induced cardiotoxicity. Front. Pharmacol. *11*, 603596. https://doi.org/10.3389/fphar.2020.603596.

31. Aubert, G., Martin, O.J., Horton, J.L., Lai, L., Vega, R.B., Leone, T.C., Koves, T., Gardell, S.J., Krüger, M., Hoppel, C.L., et al. (2016). The failing heart relies on ketone bodies as a fuel. Circulation *133*, 698–705. https://doi.org/10.1161/CIRCULATIONAHA.115.017355.

32. Bedi, K.C., Jr., Snyder, N.W., Brandimarto, J., Aziz, M., Mesaros, C., Worth, A.J., Wang, L.L., Javaheri, A., Blair, I.A., Margulies, K.B., and Rame, J.E. (2016). Evidence for intramyocardial disruption of lipid metabolism and increased myocardial ketone utilization in advanced human heart failure. Circulation *133*, 706–716. https://doi.org/10.1161/CIRCULATIONAHA.115.017545.

33. Suriben, R., Chen, M., Higbee, J., Oeffinger, J., Ventura, R., Li, B., Mondal, K., Gao, Z., Ayupova, D., Taskar, P., et al. (2020). Antibody-mediated inhibition of GDF15-GFRAL activity reverses cancer cachexia in mice. Nat. Med. *26*, 1264–1270. https://doi.org/10.1038/s41591-020-0945-x.

34. Neilan, T.G., Coelho-Filho, O.R., Pena-Herrera, D., Shah, R.V., Jerosch-Herold, M., Francis, S.A., Moslehi, J., and Kwong, R.Y. (2012). Left ventricular mass in patients with a cardiomyopathy after treatment with anthracyclines. Am. J. Cardiol. *110*, 1679–1686. https://doi.org/10.1016/j.amjcard.2012.07.040.

35. Prasad, K.M., Xu, Y., Yang, Z., Acton, S.T., and French, B.A. (2011). Robust cardiomyocyte-specific gene expression following systemic injection of AAV: in vivo gene delivery follows a Poisson distribution. Gene Ther. *18*, 43–52. https://doi.org/10.1038/gt.2010.105.

36. Agah, R., Frenkel, P.A., French, B.A., Michael, L.H., Overbeek, P.A., and Schneider, M.D. (1997). Gene recombination in postmitotic cells. Targeted expression of Cre recombinase provokes cardiac-restricted, site-specific rearrangement in adult ventricular muscle in vivo. J. Clin. Invest. *100*, 169–179. https://doi.org/10.1172/JCI119509.

37. Guo, Z., Zhang, Y., Liu, C., Youn, J.Y., and Cai, H. (2021). Toll-like receptor 2 (TLR2) knockout abrogates diabetic and obese phenotypes while restoring endothelial function via inhibition of NOX1. Diabetes *70*, 2107–2119. https://doi.org/10.2337/db20-0591.

38. Javaheri, A., Bajpai, G., Picataggi, A., Mani, S., Foroughi, L., Evie, H., Kovacs, A., Weinheimer, C.J., Hyrc, K., Xiao, Q., et al. (2019). TFEB activation in macrophages attenuates postmyocardial infarction ventricular dysfunction independently of ATG5-mediated autophagy. JCI Insight *4*, e127312. https://doi.org/10.1172/jci.insight.127312.

39. Ma, X., Liu, H., Murphy, J.T., Foyil, S.R., Godar, R.J., Abuirqeba, H., Weinheimer, C.J., Barger, P.M., and Diwan, A. (2015). Regulation of the transcription factor EB-PGC1alpha axis by beclin-1 controls mitochondrial quality and cardiomyocyte death under stress. Mol. Cell Biol. *35*, 956–976. https://doi.org/10.1128/MCB.01091-14.

40. Wang, P., Lan, R., Guo, Z., Cai, S., Wang, J., Wang, Q., Li, Z., Li, Z., Wang, Q., Li, J., et al. (2020). Histone demethylase JMJD3 mediated doxorubicin-induced cardiomyopathy by suppressing SESN2 expression. Front. Cell Dev. Biol. *8*, 548605. https://doi.org/10.3389/fcell.2020.548605.

Please cite this article in press as: Ozcan et al., Sustained alternate-day fasting potentiates doxorubicin cardiotoxicity, Cell Metabolism (2023), https://doi.org/10.1016/j.cmet.2023.02.006

STAR★METHODS

KEY RESOURCES TABLE

REAGENT or RESOURCE	SOURCE	IDENTIFIER
Antibodies		
Rabbit anti-TFEB antibody	Bethyl Laboratories	Cat#A303-673A; RRID: AB_11204751
Rabbit anti-mTOR antibody	Cell Signaling Technology	Cat#2972; RRID: AB_330978
Rabbit anti-phospho-mTOR(Ser2448) antibody	Cell Signaling Technology	Cat#5536; RRID: AB_10691552
Mouse anti-MuRF1 antibody	Santa Cruz Biotechnology	Cat#sc-398608; RRID: AB_2819249
Rabbit anti-histone H3 antibody	Cell Signaling Technology	Cat#9715; RRID: AB_331563
Rabbit anti-GAPDH antibody	Abcam	Cat#ab22555; RRID: AB_447153
Rabbit anti-β-tubulin antibody	Cell Signaling Technology	Cat#2146; RRID: AB_2210545
Anti-mouse IgG, HRP-linked Antibody	Cell Signaling Technology	Cat#7076; RRID: AB_330924
Anti-rabbit IgG, HRP-linked Antibody	Cell Signaling Technology	Cat#7074; RRID: AB_2099233
Bacterial and virus strains		
AAV9-CMV-TFEB	Maetal.[2]	N/A
AAV9-cTNT-TFEB	This paper	N/A
AAV9-shTFEB	Maetal.[2]	N/A
Chemicals, peptides, and recombinant proteins		
Doxorubicin hydrochloride (50 mg)	United States Pharmacopeia	Cat#1225703
Recombinant human GDF15 (25 μg)	Biotechne/R&D Systems	Cat#957-GD-025/CF
Critical commercial assays		
Mouse GDF15 DuoSet ELISA kit	R&D Systems	Cat#DY6385
CelLytic NuCLEAR Extraction kit	Sigma-Aldrich	Cat#NXTRACT
Deposited data		
Source data and Western blot images for manuscript figures	This paper	Data S1
Experimental models: Organisms/strains		
Mouse: C57BL/6J	The Jackson Laboratory	CAT#000664
Mouse: C57BL/6NJ	The Jackson Laboratory	CAT#005304
Mouse: MHC-Cre: Tg(Myh6-cre)1Jmk/J	The Jackson Laboratory	CAT#009074
Mouse: $TFEB^{flox}$	Trivedietal.[19]	N/A
Software and algorithms		
Graphpad Prism v9.0.2	GraphPad Software (Boston, MA)	https://www.graphpad.com/
ImageJ 1.52h	National Institute of Health	https://imagej.nih.gov/
ZEN (black edition) system 2.3	Zeiss	N/A
i-control 2.0 (for infinite reader)	TECAN	N/A
Vevo Strain	Fujifilm Visualsonics	https://www.visualsonics.com/product/software/vevo-strain-software
QMass	Medis Medical Imaging	N/A

RESOURCE AVAILABILITY

Lead contact

Further information and requests for resources and reagents should be directed to and will be fulfilled by the lead contact, Ali Javaheri (ali.javaheri@wustl.edu).

Materials availability

This study did not generate new unique reagents.

Data and code availability

All data and materials that support the findings of this study are available within the article and supplemental information. Source data and Western blot images for the figures in the manuscript are available as Data S1: Sources, related to Figures 1, 2, 3, 4, 5, 6, 7, and S1–S6. Supplemental table and figures are available as supplemental information. No new data code has been generated in this study. Any additional information required to reanalyze the data reported in this paper is available from the lead contact upon request.

EXPERIMENTAL MODEL AND SUBJECT DETAILS

Heart tissue cohort

Human heart tissue samples were available through the University of Pennsylvania Tissue Bank from three separate groups: non-failing brain dead organ donors with no clinical history of heart failure (donors) and end-stage heart failure transplant patients with clinical history of either anthracycline-induced cardiomyopathy (DC) or non-ischemic cardiomyopathy (NICM). Heart tissue was procured according to a standard protocol briefly described.[32] Briefly, all hearts underwent *in-situ* cardioplegia and were placed on wet ice. After exclusion of epicardial fat, transmural LV samples were snap frozen in liquid nitrogen and stored at -80 °C. All study procedures were approved by the University of Pennsylvania Hospital InstitutionalReviewBoard, and prospective informed consent for research use of heart tissue was obtained from all transplant recipients and next-of-kin in the case of organ donors. Given the rarity of DC hearts, donors and NICM patients were age-matched. Donors were selected who had no history of diabetes mellitus, left ventricular assist device support, or, LV mass > 300 grams.

Cardiac MRI cohort of pediatric cancer survivors

Cardiac MRI studies from survivors of pediatric cancer were obtained as part of a larger, funded, IRB approved study examining long term anthracycline cardiotoxicity in survivors of childhood cancer. A total of 30 anthracycline treated patients completed their cMRI exams, but one patient was excluded because of concurrent treatment with anti-VEGF therapy. Mean age was 16.03 ± 0.993 years, with mean years off therapy for the cohort 7.88 years, range=1.29-21.47 years. Left ventricular ejection fraction (EF), end diastolic volume (EDV), end systolic volume (ESV), stroke volume (SV), cardiac output, myocardial mass alone and indexed to body surface area (BSA) were calculated from EKG-gated steady state free precession (SSFP) sequences obtained in the short and long axes to cover the left ventricle from base to apex (TR 3.09 msec, TE1.32 msec, temporal resolution, 43.3 msec,maximum flip angle, short axis slice thickness 8 mm (20% interslice gap), long axis slice thickness 6 mm,in-plane resolution 1.8 mm, FOV by patient size. Imaging was obtained on a whole body 3.0 Tesla MRI scanner (Siemens Vida, Erlangen, Germany) with the patient placed supine using a phased-array surface coil. Analysis was performed using QMass, Medis (Leiden, The Netherlands).

Study approval

All animal studies were approved by the Animal Studies Committee at Washington University School of Medicine. Human tissue studies were deemed exempt by the Washington University School of Medicine due to the fact that only de-identified human samples were utilized, while cMRI studies were approved by the Washington School of Medicine IRB (#202002091).

Rodent studies

All murine studies were approved by the Institutional Animal Care and Usage Committee at the Washington University in St. Louis and were performed following the Guide for the Care and Use of Laboratory Animals. Wild-type mice of the C57BL/6 strain were obtained from Jackson Laboratories including C57BL/6J (males and females) and C57BL/6N (males). Mice were housed in groups of up to n=5 mice/cage and fed standard chow (Lab Diet, 5053; providing 3.4 Kcal/g with 62.1% Kcal derived from carbohydrates, 13.2% from fats, and 24.6% from protein) on a 6:00 PM to 6:00 AM dark-light cycle, in a temperature controlled specific pathogen-free facility. Alternate day fasting (ADF) was performed with total food deprivation and ad libitum access to water while mice were housed on aspen shavings-bedding from 11:00 AM to 11:00 AM of the following day to implement alternate periods of 24 h fasting and feeding, with change in bedding. Non-fasted control mice were simultaneously provided fresh food with change in aspen shavings-bedding. To measure daily food intake, we monitored the weight of the remaining food in the cage every day and averaged by mouse number. In cages with ADF, food intake on a fed day was divided by two (averaging fasted and fed days). Terminal studies on mice were initiated between 10:00 AM to 12:00 PM after an overnight period of feeding (i.e., on a fed day).

METHOD DETAILS

Reagents

Pharmacologic-grade doxorubicin hydrochloride (50 mg) was purchased from United States Pharmacopeia (Cat#1225703, USP, R11760, Rockville, MD, USA) and dissolved in 20 ml of molecular grade water to get a 2.5 mg/ml stock, stored at -80 °C,was used in all animal experiments with Dox.

Please cite this article in press as: Ozcan et al., Sustained alternate-day fasting potentiates doxorubicin cardiotoxicity, Cell Metabolism (2023), https://doi.org/10.1016/j.cmet.2023.02.006

Recombinant human GDF15 (25 μg) was purchased from Biotechne/R&D Systems (Cat#957-GD-025/CF, Minneapolis, MN, USA) and was reconstituted in 250 μl of 4 mM HCl to get a 0.1 μg/μl stock, stored at 4 °C upon reconstitution and used in all animal experiments with GDF15.

Doxorubicin cardiotoxicity studies

In age and sex-matched 8-9 weeks-old adult mice, cardiotoxicity was induced by intraperitoneal (IP) injection of Dox at specified doses. In ADF experiments, mice were randomized to ad libitum feeding or ADF, followed by vehicle or Dox 5 mg/kg once weekly x 4 weeks, at the same time each day. In mice randomized to ADF, exactly half the Dox doses were administered either after refeeding (4 hours after the onset of fasting), while the other half were administered during refeeding (4 hours after food had been provided). Echocardiography was performed as previously described,[2] and read blindly by a cardiologist. LV mass and EF were obtained using the Vevostrain package in Vevo (Fujifilm Visualsonics, Toronto, Canada). Volumetric analyses were performed using the VevoStrain speckle-tracking software included in the VevoLab workstation (Fujifilm Visualsonics, Toronto, ON, USA).[2] Pooled results from all C57BL/6 with available echocardiographic data are shown in main figures, with data from individual experiments shown in supplemental figures, as described.

Adeno-associated virus experiments

In viral transduction experiments, we employed adeno-associated virus 9 (AAV9)-driven overexpression of TFEB downstream of a cytomegalovirus promoter (mouse TFEB cDNA was cloned into a phosphorylated AAV9 vector containing the CMV cytomegalovirus promoter), as previously described.[2] C57BL/6 mice were randomized to CMV-TFEB or CMV-null control virus (3.5 x 10^{11} particles/mouse injected via tail vein), followed by vehicle or Dox. Mice treated with saline underwent echocardiography at 24 days post-viral injection along with AAV9-CMV-null Dox mice (n=5). Two AAV9-CMV-TFEB mice underwent emergency echocardiography before euthanasia due to signs of distress. In a second experiment, after two doses of Dox (5 mg/kg once weekly, IP), AAV9-CMV-null and TFEB mice were given a 3rd dose of Dox prior to planned echocardiography and euthanasia. One additional AAV9-CMV-TFEB mouse died between echocardiography and euthanasia and was therefore excluded from the analysis, although this did not affect statistical significance of our studies.

In AAV9-cTNT studies, AAV9-cTNT-HA-TFEB-p2a-GFP and GFP control were cloned into pACcTNT-mir122 vector (the luciferase was removed).[35] AAV9-cTNT-TFEB or cTNT-GFP control virus was delivered via tail vein injection as a dose of 3.5 x 10^{11} particles/mouse injected via tail vein), followed by vehicle or Dox (5 mg/kgIPx 3 doses).

In AAV9-shRNA studies, we utilized AAV9-U6-short hairpin construct to knockdown TFEB as we previously published.[2] Constructs for invivo knockdown of mouse endogenous were generated using the specific oligonucleotide sequences targeting murine TFEB (5′-CGGCAGTACTATGACTATGAT-3′); and compared with a scrambled control sequence (with no complementarity to murine genome) (5′-CCTAAGGTTAAGTCGCCCTCG-3′) by cloning into an AAV9 vector under the control of a U6 promoter. AAV9 particles were generated at the Hope Center Viral Vectors Core at Washington University School of Medicine. C57BL/6J wild-type mice were injected with AAV9-shTFEB vs AAV9-shScramble control (3.5 x 10^{11} particles/mouse injected via tail vein), followed by Dox (5 mg/kg x 2 doses, IP).

Recombinant human GDF15 experiments

Recombinant human GDF15 containing an N-terminal 6-His tag was purchased from R&D Systems (#957-GD/CF). Lyophilized protein was reconstituted with sterile 4 mM HCl and stored at 4 °C. In the first experiment, C57BL/6J mice were randomized to recombinant GDF15 (0.3 mg/kg x 6) vs 4 mM HCl (control) and treated with saline (n=3/group). In the second experiment, C57BL/6J mice were randomized to recombinant GDF15 (0.3 mg/kg SQ q3 days x 6 doses) vs 4 mM HCl (control) and treated with Dox (5 mg/kg,IPx 2 doses; n=5/group).

Cardiomyocyte-specific TFEB knockout experiments

Mice with TFEB-floxed alleles (TFEB fl/fl, Stock # 400102) deposited by Dr. Andrea Ballabio[19] were crossed with transgenic mice expressing Cre under the control of myosin heavy chain promoter[36] (MHC-Cre, Stock: 009074) to generate cardiomyocyte-specific TFEB knockout (TFEB^{CMKO}) mice, which were in a mixed C57BL/6J x 6N background. TFEB^{CMKO} and Cre negative TFEB flox (TFEB^{flox}) littermate mice randomized to vehicle (control) or Dox (5 mg/kgIPx 2 doses).

Assessment of body weight and body composition

Body weight of individual animals was measured intermittently until the end of the experimental protocol. Body composition (fat mass and lean mass) in live animals were analyzed by a rodent EchoMRI (EchoMRI LLC, Houston, TX) at the end of the experiments, as previously described.[37]

Enzyme-linked immunosorbent assay (ELISA)

A mouse GDF15 DuoSet ELISA kit (DY6385, R&D Systems, Minneapolis, MN, USA) was used to measure GDF15 levels in the sera of mice according to the manufacturers' protocol. Absorbance was measured using a TECAN infinite M200PRO plate reader and i-control microplate reader software (Tecan Trading AG, Switzerland). Absorbance at 540 nm along with 450 nm was used for correction.

Histologic analyses

Histological analyses were performed as previously described.[38] Briefly, mouse heart tissues were fixed immediately after euthanasia in 4% formalin at room temperature overnight, then stored in phosphate buffered saline (PBS) at 4 °C and embedded in paraffin wax. Paraffin sections were cut and mounted on glass slides. Images of TUNEL and Masson's trichrome-stained tissue slices of paraffin-embedded murine cardiac tissue were acquired with an Olympus BX43F light microscope. 10x images of Masson's trichrome-stained tissue slices were then quantified using the ImageJ software (National Institutes of Health). $TUNEL^+$ cells were manually counted by a blinded observer and ImageJ software was used to count all cell nuclei. High-resolution images of WGA-stained tissue slices of paraffin-embedded murine cardiac tissue were acquired using the 40x objective of a Zeiss LSM 700 confocal microscope. Cell size was measured by a blinded observer using ZEN (black edition) system 2.3.

Cytoplasmic and nuclear protein extraction

Human or mouse cardiac tissues were fractionated into nucleus-enriched and cytoplasmic samples by using a CelLytic NuCLEAR Extraction kit (Sigma, Nxtract), as previously described.[39] Briefly, myocardial tissues were mechanically homogenized for 5 minutes in isotonic buffer, provided in the kit. After 20 minutes of centrifuge, supernatants, which are cytoplasmic fractions, were transferred to new tubes and stored at -80 °C. The pellets were resuspended in isotonic buffer again and washed 2 times. After discarding the supernatants, pellets were resuspended in extraction buffer for 30 minutes. Samples were sonicated and centrifuged again for 5 minutes. Supernatants, containing the nuclear fractions, were transferred to a new tube and stored at -80 °C. Expression of proteins localized to the nucleus (histone H3) and cytoplasm (GAPDH) was examined with Western blot analysis to confirm relative enrichment.

Total protein extraction

Freshly isolated mouse heart samples were snap frozen in liquid nitrogen after sacrifice and stored at -80 °C. Tissues were homogenized in ice-cold lysis buffer (composition: 50 mM Tris HCl [pH 7.4], 2.5 mM EDTA, 10 mM EGTA, 20 mM NaF, 25 mM $Na_4P_2O_7$, 2 mM Na_3VO_4, 25 mM NaCl,and 0.2% NP-40) containing protease inhibitor cocktail (#P2714; MilliporeSigma) and then centrifuged at 12000 g for 20 min at 4 °C. After discarding the pellets, heart lysates were stored at -80 °C.

Western blot analysis

Westernblots were performed on mice or human heart tissue lysates as previously described.[40] Briefly, equal amounts of total protein (20 μg for total protein, 40 μg for nuclear protein) were separated by 4-20% SDS-PAGE and transferred onto polyvinylidene fluoride membranes (Millipore Sigma #IPVH00010). The membranes were blocked with 5% nonfat milk at room temperature for 1 h and incubated overnight at 4 °C with the primary antibodies, and the membranes were washed and further incubated with secondary antibodies at room temperature for 1 h. The immune complexes were visualized by enhanced chemiluminescent methods, and the band intensity was quantified using Image J software (National Institutes of Health). Primary antibodies employed were as follows: TFEB (Bethyl Labs, A303-673A, diluted 1:1000, Montgomery, TX, USA), phospho-mTOR (Ser2448) (Cell Signaling, #5536s, diluted 1:1000), mTOR (Cell Signaling, #2972s, diluted 1:1000), MuRF1 (Santa Cruz, #sc-398608, diluted 1:200), Histone H3 (Cell Signaling, #9715s, diluted 1:1000), GAPDH (Abcam, ab22555, diluted 1:5000, Cambridge, MA, USA) and β-tubulin (Cell Signaling, #2146s, diluted 1:1000). Secondary antibodies employed were as follows: anti-mouse IgG (Cell Signaling, #7076, diluted 1:2000), anti-rabbit IgG (Cell Signaling, #7074, diluted 1:2000).

QUANTIFICATION AND STATISTICAL ANALYSIS

When normality assumptions were confirmed, populations were compared using two-tailed Student's t-test for two groups, one-way analysis of variance (ANOVA) for three or more groups, or two-way ANOVA for comparisons of multiple parameters. Normality was visualized by Q-Q plot and confirmed by Shapiro-Wilk test. Overall ANOVA F-statistics were significant for all presented comparisons, and multiple comparisons were corrected using Sidak's test. When the residuals for a dataset with multiple parameters were not visually normal on Q-Q plots, data underwent log-transformation for the two-way ANOVA. When normality assumptions were rejected, non-parametric Mann-Whitney or Kruskal-Wallis tests were used. The log-rank test was used to compare survival distributions. Specific tests used to analyze each experiment are described in the figure legends. Data are presented as mean ±SEMunless indicated. Two-sided P values less than 0.05 were considered to be statistically significant. Statistical analyses were performed in GraphPad Prism v9.0.2 (La Jolla, CA).